Collision-induced coherence transfer studied by tunable energy compensation

J. E. Thomas
Physics Department, Duke University, Durham, North Carolina 27706

J. M. Liang and R. R. Dasari
Spectroscopy Laboratory and Physics Department, Massachusetts Institute of Technology, Cambridge, Massachusetts 02139

(Received 2 March 1990)

Collision-induced coherence transfer between infrared molecular transitions is studied using a technique that permits the complete distribution of accompanying velocity changes to be determined in a simple way. The experiments are carried out by measuring the intensity of two pulse photon echoes as a function of applied Stark field at fixed large echo time delay. The velocity change distribution for coherence-transfer collisions is obtained directly as the *shape* of the echo intensity versus Stark field curve. Previously unpublished data for dipole-quadrupole and van der Waals interactions are presented, and a theory of coherence-transfer velocity-changing kernels is developed that is in good agreement with the data.

I. INTRODUCTION

Recently we suggested and demonstrated a new method to study infrared and optical coherence transfer.[1-4] In the basic coherence-transfer process (Fig. 1), optical coherence initially created on the a'-b' transition is collisionally transferred to the a-b transition. Both the excited- and ground-state *amplitudes* of the active molecule simultaneously change in this process, accompanied by a velocity change Δv. The technique used in these studies, which we call tunable energy compensation, has been applied to measure both the rates and the distribution of velocity changes which accompany infrared coherence transfer (i.e., the one-dimensional kernel). In the experiments, coherence transfer occurs between adjacent Stark-split transitions in $^{13}CH_3F$ (Fig. 2). During coherence transfer, the excited- and the ground-state magnetic quantum numbers both change by either $\Delta M=1$ or -1, as discussed below. The coherence-transfer collision kernel $W_{\Delta M}(\Delta v)$, where Δv is the velocity change along one axis, gives the distribution of velocity changes.

The coherence-transfer kernel is obtained directly as the shape of a two-pulse photon echo intensity I_e versus Stark-field curve, at fixed large echo time delay T. The method works by singling out those collisions for which the collision-induced Doppler shift is compensated by the tunable Stark frequency change which accompanies infrared coherence transfer in the applied Stark field.

For $^{13}CH_3F$, which has a large permanent electric dipole moment, collisions with perturbers with permanent multipole moments predominantly cause infrared coherence transfer between adjacent transitions (see Fig. 2) which differ in magnetic quantum number by an amount ΔM, obeying dipole selection rules: $\Delta M=0,\pm1$. In this case, the (initial-M-averaged) one-dimensional kernel for velocity change Δv and coherence transfer with $|\Delta M|=1$ is obtained from the echo data in the remarkably simple form[1-4]

$$\mathrm{Re}W_{|\Delta M|=1}(\Delta v)=\frac{1}{4\lambda}\ln\frac{I_e(\nu_s=\Delta v/\lambda)}{I_e(\nu_s\rightarrow\infty)}\ , \tag{1}$$

where the kernel is in units (rad/s)/(cm/s). The delay time T is taken sufficiently long that $T\gg\lambda/(2\pi\Delta v)$, where λ is the infrared transition wavelength. It is as-

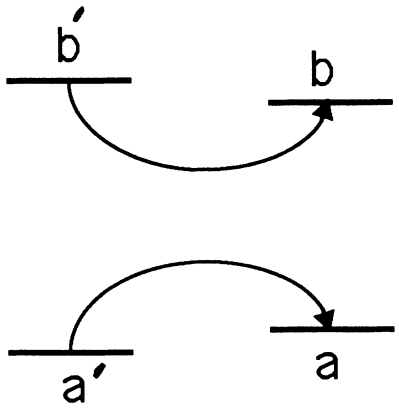

FIG. 1. Coherence-transfer process.

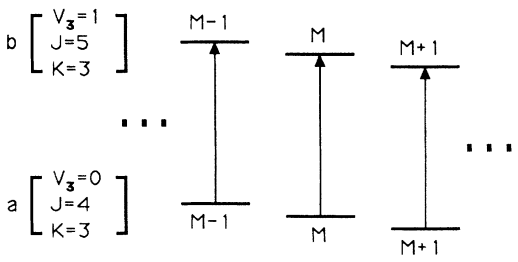

FIG. 2. Energy levels and transitions in a weak dc Stark field.

sumed that the laser field and the Stark field are $\hat{\mathbf{z}}$ polarized. ν_s is the *transition* Stark frequency shift (Hz) per unit M (i.e., the excited-state shift minus the ground-state shift at $M=1$) which is linearly proportional to the Stark voltage. Finally, the laser pulse bandwidth is assumed large compared to both the transition Stark shifts and the collision-induced Doppler shifts.

Physically, Eq. (1) is easy to understand. At large echo time delay, $T \gg \lambda/(2\pi\Delta v)$, the random collision-induced Doppler shifts $\Delta v/\lambda$ (Hz units) tend to destroy the macroscopic polarization and hence reduce the echo signal. However, in the Stark field, collision-induced coherence transfer between adjacent transitions differing in magnetic quantum number by 1 ($\Delta M=1$) causes an additional frequency change $\Delta M\nu_s$. In this case, collisions for which $\Delta v/\lambda+\Delta M\nu_s=0$ cause no net frequency change of the oscillator, thereby eliminating the echo degradation due to the velocity change Δv. The "probability" of these energy-compensated collisions occurring, which determines $\ln I_e$ is the order of the time scale of the echo experiment T, times the rate at which such collisions occur. The rate is the order of the product of the coherence-transfer velocity-changing kernel $W_{\Delta M}(\Delta v=\lambda\Delta M\nu_s)$ (rate per unit velocity for coherence transfer between adjacent transitions differing in magnetic quantum number by ΔM with velocity change Δv) times the velocity resolution for the echo experiment $\lambda/(2\pi T)$. Since the time T cancels in the "probability," the kernel and $\ln I_e$ are directly proportional in the large-T limit.

An important feature of this technique is that the kernels are obtained on an *absolute* scale, trivially. Hence, the shapes of the kernels, for example, the values of the kernels at zero velocity change, are readily obtained for comparison with theory.

Infrared and optical coherence-transfer collisions are described by the quantum-transport equation[5–7] and have in principle been known for some time. However, the conditions under which collision-induced coherence transfer can occur are not well established and have only recently been investigated experimentally. The work described in this paper and Refs. 1–4 are the only studies, we believe, which explore the correlation between coherence transfer and the accompanying velocity changes. Processes of this type have been analyzed theoretically in some detail with neglect of the accompanying velocity changes.[8,9] Previous experiments have studied collision-induced Zeeman coherence and microwave coherence rotational transfer (intramolecular), for which velocity changes were not measured.[10] Studies of the Stark-splitting dependence of the line-broadening rates,[11] also involve coherence transfer between transitions differing in magnetic quantum numbers, but the accompanying velocity change distributions have not been measured.

In this paper, we exploit Eq. (1) to measure the velocity-changing kernels for $^{13}CH_3F$-$^{12}CH_3F$ (dipole-dipole) and $^{13}CH_3F$-CO_2 (dipole-quadrupole) coherence-transfer collisions. Results for $^{13}CH_3F$-Ar (van der Waals) collisions are also described. Briefly, the organization of this paper is as follows. Section II reviews the theory of echo formation in a weak Stark field to derive Eq. (1). The experiments are discussed in Sec. III, where experimentally measured kernels are presented. In the Appendix, average one-dimensional coherence-transfer kernels are derived from first principles and evaluated within the framework of a simple model. The model kernels are compared to the data in Sec. IV. Finally, a discussion of why phase disruption does not preclude collision-induced coherence transfer in this system is presented in Sec. V.

II. THEORY

A. Echo formation without collisions

We consider first the excitation of a high-J molecular transition in the absence of collisions, assuming a $\hat{\mathbf{z}}$-polarized excitation laser field of the form

$$\mathbf{E}(x,t)=\tfrac{1}{2}\hat{\mathbf{z}}E_0(t)e^{i(qx-\omega t)}+\text{c.c.}\ , \tag{2}$$

where the infrared wave vector is $q=2\pi/\lambda$ and $\omega=cq$. In this case, transitions between the ground vibrational state a and the excited vibrational state b occur between all pairs of states with identical magnetic quantum number M (Fig. 2). For R branch lines ($J_b=J_a+1$) there will be $2J_a+1$ independent transitions ($-J_a\le M\le J_a$), three of which ($M,M'=M\pm1$) are shown in the figure. Now we apply a small $\hat{\mathbf{z}}$-polarized dc electric field E_s to the sample molecules, which are assumed to be symmetric top molecules with a permanent dipole moment. Then, the infrared transition frequency ω_{ba} is shifted by[12]

$$\omega_s M\equiv-\frac{E_s}{\hbar}K\left[\frac{\mu_b}{J_b(J_b+1)}-\frac{\mu_a}{J_a(J_a+1)}\right]M\ , \tag{3}$$

where K is the projection of the molecular angular momentum on the molecular symmetry axis. Note that we use states of definite K which diagonalize the Stark-field interaction rather than states of definite parity. The shift given by Eq. (3) is just the difference between the excited b and ground-state a first-order Stark shifts. Each transition resonance frequency is shifted by an amount proportional to M so that Eq. (3) defines the Stark shift per unit M, $\omega_s=2\pi\nu_s$. For vibrational transitions, the permanent dipole moments μ_a and μ_b differ by only about 1% (Ref. 12) and the primary contribution to Eq. (3) is due to the difference between the rotational quantum numbers J_b and J_a.

In order to generate a two-pulse echo in a gaseous medium, two short excitation pulses, separated by a time delay T, are used to excite the sample. An echo pulse is then emitted at time $2T$ after the first pulse.[13] As is well known,[13] in a vapor-phase echo experiment the first pulse produces an array of radiating dipoles which are initially in phase, exhibiting an oscillating macroscopic dipole moment. This dipole moment quickly undergoes Doppler dephasing due to the inhomogeneous translational motion. A second pulse conjugates the polarization, thereby reversing the dephasing process, leading to the buildup of a macroscopic polarization in the medium at time $2T$, which generates the echo signal.

In the present experiments, the macroscopic dipole

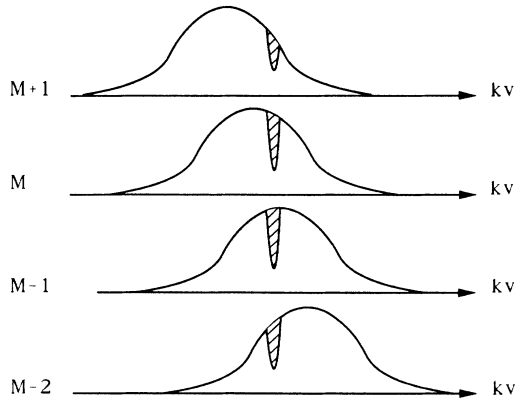

FIG. 3. Overlapping doppler profiles for Stark split transitions.

moments for each of the independent transitions shown in Fig. 2 undergo the same dephasing-rephasing process described above, leading to echo formation at a time $2T$ after the first pulse. It is interesting to note, however, that even if the all of the molecules were at rest (no Doppler dephasing), an echo signal would still arise when a small Stark field is applied. This is due to the M dependence of the frequency shift, Eq. (3), which results in an effective frequency inhomogeneity. The dipoles for transitions of different M radiate different frequencies which dephase and rephase exactly as in the Doppler-broadened case.

An important feature of the experiments described in this paper is that they employ excitation pulse bandwidths and transition Stark frequency shifts which are small compared to the Doppler width. This has the consequence, as shown in Fig. 3, that the echo field emitted by the radiating dipoles for each M transition has a center frequency equal to that of the excitation laser field ω. Hence, no beating phenomena are expected in the absence of collisions[14] and the peak echo intensity at time $2T$ will be independent of Stark field in this case. This is in contrast to some sublevel and quantum beat experiments.[15]

B. Coherence-transfer collisions

As suggested in the above discussion, in the presence of a Stark field, the M dependence of the transition frequency for a high-J system leads to an effective frequency inhomogeneity in addition to the usual Doppler inhomogeneity. By analogy to the echo techniques which have been developed to study vapor-phase velocity-changing collisions, a variety of new techniques can be developed to study molecular coherence-transfer velocity-changing kernels, using for data analysis approximations similar to those applied previously for elastic velocity-changing collisions. In this section, we exploit this analogy to develop techniques to study infrared coherence-transfer velocity-changing kernels, and present a theory of echo formation in the presence of coherence transfer.

The echo intensity is proportional to the square of the macroscopic polarization when the echo occurs at time $2T$ relative to the first input pulse in the echo experiment as described above. For $\hat{\mathbf{z}}$-polarized laser excitation, the macroscopic molecular polarization $\mathbf{P}$ is given by

$$\mathbf{P}=\hat{\mathbf{z}}\,\mathrm{Re}2\sum_{M}\int dv\,\mu_{ab}(M)\rho_{ab}(M,v,t)\ , \tag{4}$$

where $\mu_{ab}(M)$ is the infrared or optical transition dipole moment between states a and b for magnetic quantum number M. $\rho_{ba}(M,v)$ is the corresponding density matrix element for atoms with velocity component v along the laser field propagation direction $\hat{\mathbf{x}}$. In the absence of collisions, the polarization dephasing and rephasing processes described above lead to an echo at a time $2T$ relative to the first input pulse.

The collisional evolution of the echo signal versus time delay T can be derived from the equation of motion for $\rho_{ba}(M,v,t)$ with the laser field off, assuming that the input pulses are of short duration compared to the time in between pulses. Assuming spherically averaged kernels (see the Appendix),[16] and using the kernel abbreviations given in Eq. (6) below, the coherence evolution due to collisions is given by

$$\begin{aligned}\left[\frac{\partial}{\partial t}+v\frac{\partial}{\partial x}\right]\rho_{ba}(M,v)=&-i(\omega_{ba}+\omega_s M)\rho_{ba}(M,v)\\&-\Gamma_M(v)\rho_{ba}(M,v)\\&+\sum_{M'}\int dv W_{M\leftarrow M'}(v\leftarrow v')\\&\times\rho_{ba}(M',v')\ .\end{aligned} \tag{5}$$

In writing Eq. (5), we assume that the perturber pressure is low enough that collisional evolution during the laser pulses is negligible compared to that occurring in the time delay T in between the pulses. The right-hand side of Eq. (5) contains the infrared or optical transition frequency ω_{ba} which is shifted for each M (Fig. 2) due to the applied Stark field by $\omega_s M$, according to Eq. (3). The rate $\Gamma_M(v)$ is the *total* coherence loss rate due to inelastic collisions (J changing, etc.), elastic coherence-transfer between transitions, $M\rightarrow M'\neq M$, and elastic velocity changes $M\rightarrow M$ and $v\rightarrow v'$. The spontaneous rate also can be included, but is negligible in the present experiments. The kernels $W_{M\leftarrow M'}(v\leftarrow v')$ describe the rate per unit velocity for velocity change $v'\rightarrow v$ with *coherence transfer* between *transitions* labeled by M' and M (Fig. 2). Generally, as shown in the Appendix, the kernels are four index quantities describing coherence transfer between pairs of transitions $(a',b')\rightarrow(a,b)$, as depicted in Fig. 1. However, since we choose $\hat{\mathbf{z}}$-polarized laser excitation, and impose approximate spherical symmetry on the kernels, levels a and b have the same magnetic quantum number M, and levels a' and b' must have the same magnetic quantum number M' (i.e., the ground- and excited-state amplitudes must reorient by the same amount $\Delta M=M-M'$ in a spherically symmetric approximation). The rather cumbersome notation for the four index kernels is therefore abbreviated using

$$W^{bM\leftarrow bM'}_{aM\leftarrow aM'}(v\leftarrow v')\equiv W_{M\leftarrow M'}(v\leftarrow v')\ . \tag{6}$$

The total loss rate $\Gamma_M(v)$ has been similarly abbreviated.

It is convenient to eliminate the collision-free evolution from Eq. (5) by defining

$$\rho_{ba}(M,v,t)=d_M(v,t)e^{i(\omega-\omega_{ba}-qv-\omega_s M)t}e^{i(qx-\omega t)} . \quad (7)$$

In the limit of velocity selective excitation, of interest in the present experiments, the functions $d_M(v,t)$ are peaked for v such that $\omega-\omega_{ba}-qv-\omega_s M=0$. Hence the center frequency of $\rho_{ba}(M,v,t)$ is equal to that of the laser ω and is independent of M, as discussed above. Hence no beating phenomena occur in the absence of collisions. [By contrast, for broadband excitation of the entire Doppler profile, the d_M functions peak at $v=0$ and each Stark shifted component, $\rho_{ba}(M,v,t)$ radiates at a different frequency, leading to beats.] By substituting Eq. (7) for ρ_{ba} into the evolution equation (5), the d_M functions are found to obey[1]

$$\dot{d}_M(v,t)=-\Gamma_M(v)d_M(v,t)+\sum_{M'}\int dv' W_{M\leftarrow M'}(v\leftarrow v')\times e^{i[q(v-v')+\omega_s(M-M')]t}d_{M'}(v',t) . \quad (8)$$

The one-dimensional kernels $W_{M\leftarrow M'}(v\leftarrow v')$ take the form of Eq. (29) as obtained from isotropically averaged three-dimensional kernels, Eq. (27), and so depend only on $|\Delta v|=|v-v'|$. Equation (8) shows that the arrival term for the coherence oscillates in time due to the phase $[q(v-v')+\omega_s(M-M')]t$. Physically, the oscillation arises because at certain times, adjacent transitions initially excited at $t=0$ have the same phase, and collisional transfer of coherence at such times adds constructively.

An analytic solution to Eq. (8) can be obtained with the following fairly general simplifying assumptions:[1] (i) an excitation bandwidth much larger than the Stark shifts accompanying collision induced coherence transfer $(M-M')\omega_s$ and associated Doppler shifts $q(v-v')$, as well as all decay rates; (ii) a velocity selective excitation with v' small compared to the perturber speed so that the kernel is symmetric in Δv for the small-angle collisions which the coherence survives without destruction due to inelastic processes [see discussion following Eq. (26) in the Appendix]; (iii) a high J limit so that both $d_{M'}$ and $W_{M\leftarrow M'}$ are slowly varying functions of M' for the transitions which contribute most to the echo signal. Further, we assume that coherence transfer occurs between transitions differing in magnetic quantum only by $\Delta M \ll J$. In this case, the kernels can be averaged over initial M' values holding $\Delta M=M-M'$ constant, yielding one-dimensional kernels according to Eqs. (29) and (62) which are functions of $|\Delta M|$ and $|\Delta v|$ only. Further, in this approximation, $d_{M'}\simeq d_M$ and $\Gamma_M(v)\simeq\Gamma$. With these assumptions, the slowly varying echo polarization at time $2T$ is readily obtained from Eq. (8) as

$$d_M(2T)=d_M(0)e^{-2\Gamma T}\times\exp\left[-\sum_{\Delta M}\int_0^T dt\int_{-\infty}^{\infty}d(\Delta v)W_{\Delta M}(\Delta v)\times e^{-i(q\Delta v+\omega_s\Delta M)t}+\text{c.c.}\right] . \quad (9)$$

The complex-conjugate term in the exponent of Eq. (9) arises from the polarization conjugation at time T due to the second input pulse in the echo experiment. The first term in the exponent arises from the collisional evolution between T and $2T$ with the substitution $t'=t-T$ in the frequency-dependent phase. All coherences with different orientations M have the same decay function within the framework of the above approximations. The echo signal intensity, which is proportional to the square of the macroscopic polarization, is then obtained in the form

$$I_e(2T)=I_e(0)e^{-4\Gamma T}\times\exp\left[-2\sum_{\Delta M}\int_0^T dt\int_{-\infty}^{\infty}d(\Delta v)W_{\Delta M}(\Delta v)\times e^{-i(q\Delta v+\omega_s\Delta M)t}+\text{c.c.}\right] . \quad (10)$$

As a function of the delay time T a collision-induced *oscillatory* echo decay curve $\ln I_e(2T)/I_e(0)$ arises, containing a frequency component $\omega_s\Delta M$ for each coherence-transfer kernel $W_{\Delta M}$ according to this result. If ω_s is chosen to be larger than the average collision-induced Doppler shift $q\Delta v$, Fourier transformation of the slope of $\ln I_e(\omega_s,T)$ versus T at fixed ω_s can be used to obtain *all* of the *kernels*, including $\Delta M=0$ as a series of peaks with separation ω_s. The shape of each peak shifted from $\Delta M=0$ by $\Delta M\omega_s$ is the kernel $W_{\Delta M}(\Delta v)$.

In this paper, we consider an alternative experiment, namely, we measure the curves obtained by varying ω_s at fixed time delay T.[1-4] It is particularly convenient to measure the ratio of the echo intensity with the Stark field off ($\omega_s=0$) and on ($\omega_s\neq 0$), so that all voltage-independent collisions are suppressed, and pure coherence-transfer collisions with $\Delta M\neq 0$ are isolated for study. Using the symmetry of the kernels in ΔM and Δv, one obtains from Eq. (10) for fixed T

$$\ln\frac{I_e(\omega_s=0;T)}{I_e(\omega_s;T)}=16\,\mathrm{Re}\sum_{\Delta M>0}\int_0^{\infty}d(\Delta v)W_{\Delta M}(\Delta v)\int_0^T dt\cos(q\Delta v t)[1-\cos(\Delta M\omega_s t)] . \quad (11)$$

As a function of ω_s, Eq. (11) shows that an oscillatory curve is again obtained containing a frequency component for each coherence-transfer kernel. The kernels and hence the curves are linearly proportional to perturber gas pressure and are independent of the sample's absorption coefficient, the detector efficiency,

amplification, spontaneous decay, and transit time decay which normally affect echo versus time delay signals.

When one kernel for some given $\Delta M \neq 0$ is dominant, Eq. (11) can be dramatically simplified in the large time delay limit. For $^{13}CH_3F$ collisions with molecular perturbers having permanent multipole moments, the permanent dipole interaction of the active molecule implies the selection rule $\Delta M = 0, \pm 1$ for $^{13}CH_3F$ infrared coherence transfer (see the Appendix). Hence, only one term, with $|\Delta M| = 1$ in Eq. (11) is nonzero. In this case, the dominant kernel (with $|\Delta M| = 1$) can be obtained directly from the data. Mathematically, the time integral in Eq. (11) yields δ functions in the limit $T \to \infty$ $[T \gg 1/(q\Delta v)]$,

$$\int_0^\infty dt \cos(q\Delta v t)[1-\cos(\Delta M \omega_s t)] = \frac{\pi}{2}[\delta(q\Delta v)-\delta(q\Delta v + \Delta M \omega_s)] , \quad (12)$$

valid for positive values of the δ-function arguments. Then, retaining only the dominant kernel for one value of ΔM, Eq. (11) takes the form

$$\ln \frac{I_e(\omega_s = 0)}{I_e(\omega_s)} = \frac{8\pi}{q} \mathrm{Re}\left[W_{\Delta M}(0) - W_{\Delta M}\left[\Delta v = \frac{\Delta M \omega_s}{q} \right] \right] . \quad (13)$$

For large $\omega_s \to \infty$ (i.e., $\gg q\Delta v_{\max}$), the second term on the right-hand side of Eq. (13) is $W_{\Delta M}(\Delta v \to \infty) \to 0$. Hence

$$\mathrm{Re} W_{\Delta M}(0) = \frac{q}{8\pi} \ln \frac{I_e(\omega_s = 0)}{I_e(\omega_s \to \infty)} .$$

Using this in Eq. (13), one obtains

$$\mathrm{Re} W_{\Delta M}(\Delta v) = \frac{q}{8\pi} \ln \frac{I_e(\omega_s = q\Delta v / \Delta M)}{I_e(\omega_s \to \infty)} , \quad (14)$$

where $\Delta M > 0$ and $T \gg 1/(q\Delta v)$. With $q = 2\pi/\lambda$ and $\omega_s = 2\pi\nu_s$, Eq. (14) reproduces Eq. (1) for $\Delta M = 1$.

Equation (14) shows that a simple plot of echo intensity (ln scale) versus Stark voltage at fixed large time delay T yields the kernel directly relative to the baseline, $\ln I_e(\omega_s \to \infty)$. The limit $T \to \infty$ is readily ascertained by measuring curves for different T and noting when the curve no longer changes shape as T is increased. The abscissa unit is scaled to cm/s according to $\Delta v = \Delta M \nu_s \lambda$ and the ordinate is scaled by $1/(4\lambda)$ to units of [(rad/s)/Torr]/(cm/s) after dividing the measured logarithms by the perturber pressure in Torr. Twice the area under the scaled data curve (integral of the velocity change distribution) gives the coherence-transfer rate for the dominant ΔM.

A particularly important feature of Eq. (14) is that it yields kernels directly from data in *absolute* units, assuming only that the Stark tuning frequency ω_s, transition wavelength λ, and perturber pressure are accurately known. Hence the value of $W_{\Delta M}$ $(\Delta v = 0)$ is measured along with the kernel shape, width, and total rate for coherence transfer between transitions differing in magnetic quantum number by ΔM.

In the following section, coherence transfer is studied using Eq. (1) for collisions between $^{13}CH_3F$ and $^{12}CH_3F$, CO_2, or Ar perturbers. The results are compared to the model theoretical predictions given in the Appendix and summarized in Sec. IV.

III. EXPERIMENT

The experimental arrangement employed throughout this work is shown in Fig. 4.[1-4] Acousto-optic (AO) intensity modulation of continuous wave (cw) CO_2 laser radiation is used to generate the input pulses for the echo experiments. The laser frequency is locked to the side of its own gain profile so that both frequency and intensity are very stable. During the input pulses, a second AO modulator acts as a blinder and protects the detector. This AO is turned on just after the two input pulses to let the echo signal reach the detector. Reproducible input pulse generation with a repetition rate of 20 kHz is achieved with this technique. A novel digitally controlled TTL oscillator is employed to replace the commercial oscillator which drives the AO modulators.[1-4] There is no rf leakage between input pulses, since the oscillator is disabled during that period, so that the on/off rejection ratio of the AO is scattered light limited at 10^6:1, yielding echoes with very high signal-to-background ratio (Fig. 5).

In the experiments, a dc Stark field is applied over the length of a 1.4-m absorption cell by means of two parallel aluminum plates 5.1 cm wide and 2.54 ± 0.003-cm spacing. These give a uniform field over the 1-cm^2 laser spot size. A wire grid infrared linear polarizer is placed just before the input to the cell to make the laser polarization parallel to the Stark field. Any small Stark-field inhomogeneity does not affect the echo signal because the rephasing process removes all inhomogeneous dephasing. The effects of the Stark-field inhomogeneity on collision-induced signals were investigated and found to be unimportant.[1-4]

The molecule $^{13}CH_3F$ is chosen for the experiments because of its strong $R(v_3, J=4, K=3)$ coincidence with the $9P(32)$ CO_2 laser line at 1035.47 cm^{-1}.[17] The large K/J ratio and strong permanent dipole moment give this molecule the advantage of being easily tipped by long-

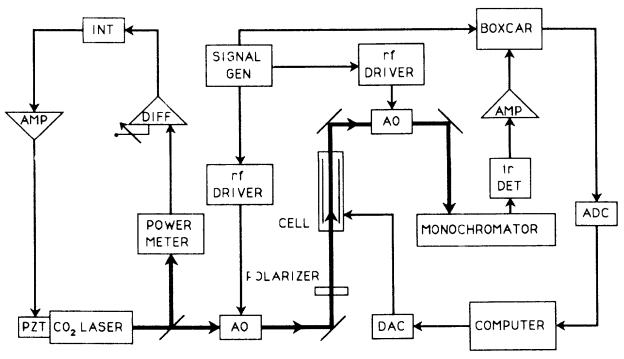

FIG. 4. Experimental arrangement.

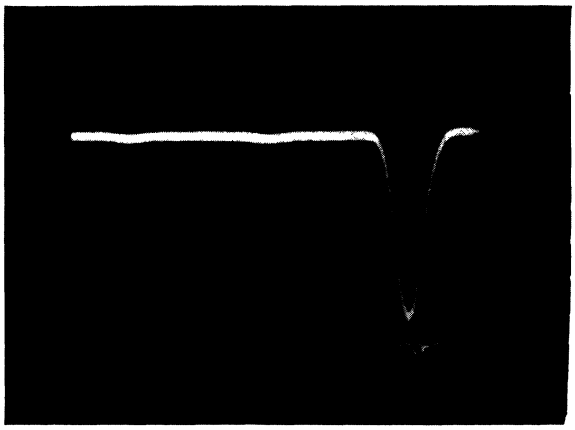

FIG. 5. Echo signal.

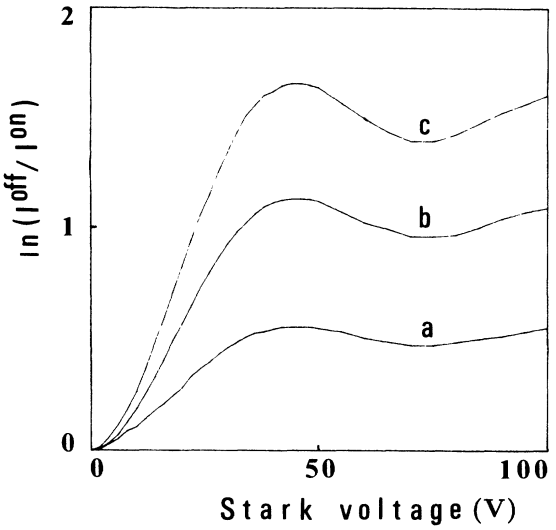

FIG. 6. Echo intensity vs Stark field for methyl fluoride perturbers at $2T=2$ μs. $^{13}CH_3F$ pressure fixed at 3.9 mTorr. Curves a, b, and c represent the total pressure of $^{13}CH_3F+^{12}CH_3F$: 3.9, 7.9, and 11.6 mTorr, respectively.

range anisotropic dipole-multipole collision potentials. According to Eq. (3), the *transition* Stark tuning rate for $\hat{z}$-polarized laser excitation is $(\omega_s/2\pi V)=17.5$ kHz/V for unit M using the Stark plates described above.

The experiments are performed quite simply by recording the echo intensity versus Stark field at fixed time delay T between the input pulses. The peak echo intensity is monitored using a boxcar (10-ns gate), the output of which is sent to a microcomputer. The microcomputer is used to scan a Kepco power supply from 0–100 V with a 0-V output between every two voltage points. In this way, the ratio of the echo intensity with the Stark field on and off can be directly measured in the experiments, eliminating the need to determine signal attenuation and gain changes.

$^{13}CH_3F$ and perturber pressures are measured using an MKS capacitance manometer (Model 390, 1-Torr range). The $^{13}CH_3F$ gas sample is supplied by MDISOTOPES and is 90% enriched.

This system has been applied to study $^{13}CH_3F$ coherence-transfer collisions and to determine the distribution of accompanying velocity changes (i.e., the kernel) for the perturbers $^{12}CH_3F$, CO_2, and Ar. In this way, dipole-dipole, dipole-quadrupole, and van der Waals interactions are studied.

A. Coherence transfer by dipole-dipole collisions

Dipole-dipole collisions are studied using methyl fluoride as a perturber. Figure 6 shows the signals obtained for $^{13}CH_3F$ self-collisions as well as for $^{13}CH_3F$-$^{12}CH_3F$ collisions. For the latter case, $^{12}CH_3F$ does not interact with the laser pulses and introduction of $^{12}CH_3F$ causes the echo intensity to drop both with the Stark field on (I^{on}) and off (I^{off}), but $\ln(I^{off}/I^{on})$ *increases linearly* with perturber pressure.[1–4] This is exactly as predicted according to Eq. (11). Identical curves are obtained for pure $^{13}CH_3F$ at the same total pressure as expected, since the permanent dipole moments are almost identical for $^{12}CH_3F$ and $^{13}CH_3F$. Note that the dependence of the echo intensity on the laser absorption coefficient cancels out in the ratio I^{off}/I^{on} so that only collisional effects are studied. The oscillatory curves obtained in Fig. 6 are of the form expected if $|\Delta M|=1$ coherence-transfer collisions are dominant (i.e., only one Fourier component is present). Note that $\Delta M=0$ and inelastic collisions are Stark-field independent and do not contribute to the signal when the ratio I^{off}/I^{on} is taken.

Since the coherence-transfer collisions with $|\Delta M|=1$ are dominant, Eq. (1) shows that the distribution of velocity changes accompanying the coherence transfer can be obtained directly from the shape of the echo intensity versus Stark voltage curve at fixed large time delay T where the shape is independent of T. Figure 7 shows how the shape of this curve evolves from oscillatory (a,b,c) to the kernel shape (d or e) which is T independent. Note

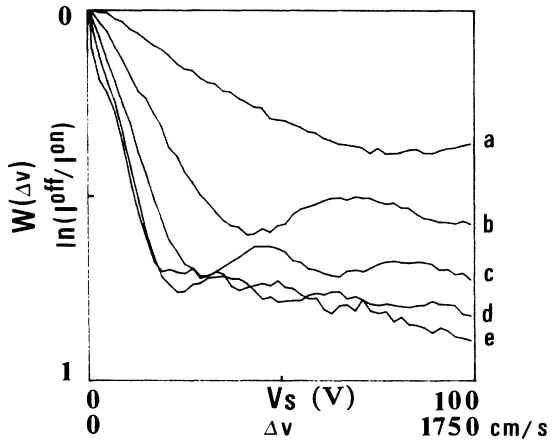

FIG. 7. Variation of echo intensity with time delay. The shape of the curve approaches that of the coherence-transfer kernel at large T. Curves a, b, c, d, and e; $2T=1$, 2, 3, 4, and 5 μs, respectively. Full vertical scale: $\ln(I^{off}/I^{on})=242$ Torr^{-1}, $W_{\Delta M=1}(\Delta v)=10.0$ [(kHz/Torr)/(cm/s)].

that if velocity changes did not occur, the oscillatory curve amplitudes would increase *linearly* with T. To obtain the kernel, the horizontal scale is transformed to cm/s using Eq. (1), $\Delta v = \lambda \nu_s$, where the transition Stark tuning rate is $\nu_s = 17.5$ kHz/V. The vertical scale is transformed from Torr^{-1} to [(rad/s)/Torr]/(cm/s) by the factor $(4\lambda)^{-1}$ in Eq. (1). (Dividing by an additional factor of 2π converts the rad/s unit to Hz units.) Note that the baseline for the kernel is approximately the horizontal line through the asymptote of curves d or e. The results of the measurements are discussed in Sec. IV, where the experimental and theoretical kernels and rates are compared.

B. Coherence transfer by dipole-quadrupole collisions

Introducing CO_2 as a perturber with no permanent dipole moment and a large quadrupole moment, we investigate dipole-quadrupole collisions. Since the active molecule $^{13}CH_3F$ is expected to exhibit dipole selection rules, Eq. (1) can be used to obtain the kernel for coherence transfer in this case also. Figure 8 shows the result of adding CO_2 gas to $^{13}CH_3F$. The $^{13}CH_3F$ pressure is fixed at 1.4 mTorr, and CO_2 is added up to 30 mTorr. The echo intensities of both I^{off} and I^{on} (Stark field off or on) are degraded by the J-changing destruction rate of about 7 MHz/Torr.[18] However, $\ln(I^{\text{off}}/I^{\text{on}})$ increases linearly with CO_2 pressure. The coherence transfer due to CO_2 collisions can be singled out by subtracting the data curve

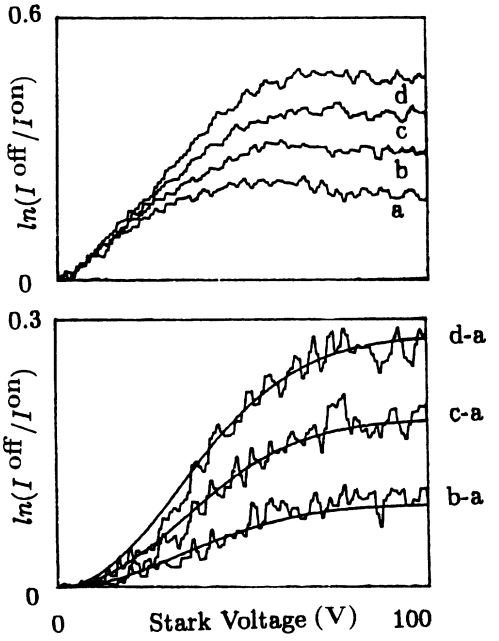

FIG. 8. Echo intensity vs Stark voltage for CO_2 perturbers at $2T = 1.5$ μs. Curve a: Pure $^{13}CH_3F$ at 1.4 mTorr. Curves b, c, and d: total $^{13}CH_3F + CO_2$ pressure of 10, 20, and 30 mTorr, respectively. Lower curves show the effect of CO_2 by subtracting the pure $^{13}CH_3F$ data. These curves show the shape of the coherence-transfer kernel for CO_2 perturbers plotted upside down.

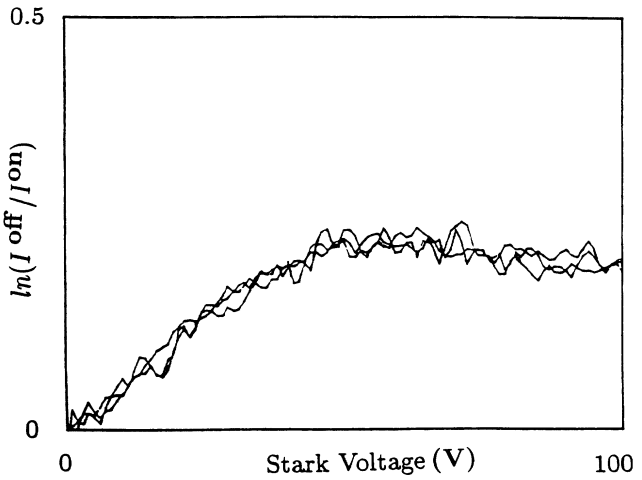

FIG. 9. Echo intensity vs Stark voltage for argon perturbers at $2T = 1.5$ μs. Three curves are plotted: pure $^{13}CH_3F$ at 2 mTorr and $^{13}CH_3F + Ar$ at total pressures of 23.5 and 13.2 mTorr. All three curves coincide within the signal-to-noise ratio showing that argon is ineffective at inducing coherence transfer in this case.

with pure $^{13}CH_3F$ from those with CO_2 as shown in the lower curves of Fig. 8. At an echo formation time of $2T = 1$ μs, the oscillation caused by the coherence transfer still remains in the CO_2 collision curves, analogous to Fig. 7(b). As $2T$ is increased to 1.5 and 2 μs, the oscillation disappears in the data curves, and the long-time curves have identical shape and height. Hence, the lower Fig. 8 curves (d−a), which subtract out the effect of $^{13}CH_3$ self-collisions, give the kernel shape plotted upside down. The kernel full vertical scale is $0.28/[(30-1.4)\ \text{mTorr}] = 9.66\ \text{Torr}^{-1}$ which is equivalent to 0.40 (kHz/Torr)/(cm/s) by scaling with $1/(8\pi\lambda)$. The horizontal full scale is 1750 cm/s, since the transition Stark frequency shift ν_s is unchanged from the dipole-dipole experiment. The kernel shape and collision rates are discussed in Sec. IV.

C. Coherence transfer by van der Waals collisions

For rare-gas perturbers, there are no permanent moments and the lowest-order interaction with the active methyl fluoride molecule is the dipole-induced-dipole or van der Waals force. Figure 9 shows the result of adding up to 23.5 mTorr of argon gas to $^{13}CH_3F$ at a fixed partial pressure of 2 mTorr. There is no measurable change in the $\ln(I^{\text{off}}/I^{\text{on}})$ signal even though the echo intensities degrade at the argon line-broadening rate of 3 MHz/Torr,[19] more than a factor of 3 in the experiment. Hence, the van der Waals force is not effective in causing coherence transfer in this system, compared to the inelastic rates which destroy the coherence. This is discussed further in Sec. IV.

IV. COHERENCE-TRANSFER COLLISION KERNELS

In this section, we compare the coherence-transfer kernels obtained from the experiments with those derived using a model which is described in detail in the Appendix

TABLE I. Molecular collision parameters.

Perturber	Multipole moment	Line-broadening rate
CH_3F	$\mu_0 = 1.86 \times 10^{-18}$ esu cm[a]	15.5 MHz/Torr[b]
CO_2	$Q_{zz} = 8.6 \times 10^{-26}$ esu cm^2[c]	7 MHz/Torr[c]

[a]Reference 12.
[b]Reference 20.
[c]Reference 18.

and summarized briefly here. The model assumes that for the small-angle collisions of interest here, coherence-transfer interactions occur only for long-range active molecule-perturber encounters *outside* of some minimum radius b_m. Inside this radius, it is assumed that inelastic processes (for example, J-changing interactions) dominate and the coherence is destroyed rather than transferred. The destruction radius b_m is determined from the known coherence destruction rate (i.e., the line-broadening rate). For simplicity, the perturber final states are limited to those corresponding to elastic scattering in the calculation of the coherence-transfer rates. It is assumed that for an interaction where the perturber inelastically scatters, the active molecule also would inelastically scatter, destroying the coherence. This assumption, which leads to good agreement with experiment, limits the maximum coherence velocity changes for which the theory is valid to those which are small enough that energy conservation prohibits inelastic perturber scattering: the maximum possible translational energy transfer must be lower than the threshold for perturber inelastic collisions. Note that the active molecule must scatter elastically for transfer of coherence between magnetic substates as studied here. We examine the threshold condition for inelastic scattering in each case below. Scattering amplitudes are calculated by taking the $\hat{z}$ axis in the collision frame to be along the initial relative velocity and using a simple first Born approximation with the minimum impact parameter limited to b_m. This ensures convergence of the integrals. The theory does not apply to elastic $\Delta M=0$ scattering because shadow scattering (which arises from inelastic processes) is not included in the theory for the region of impact-parameter cutoff below b_m. Finally, it is assumed that the dominant potential is the permanent multipole potential. The effect of other potentials, such as scalar van der Waals, on the trajectories is not included. It is assumed that they are of shorter range, and hence do not affect the calculated velocity changes. With these assumptions, the one-dimensional initial M' averaged kernels are determined. The spherical averaging and isotropic approximations used to simplify the results are described in the Appendix. The one-dimensional kernels take the following simple forms: For dipole-dipole scattering, Eq. (73) is

$$W^{d-d}_{|\Delta M|=1}(\Delta v)=\gamma^{d-d}_{|\Delta M|=1}\frac{2}{\delta v}\int_{2|\Delta v|/\delta v}^{\infty} dy \left[\frac{J_1(y)}{y}\right]^2 , \quad (15)$$

and for dipole-quadrupole scattering, Eq. (81) is

$$W^{d-Q}_{|\Delta M|=1}(\Delta v)=\gamma^{d-Q}_{|\Delta M|=1}\frac{4}{\delta v}\int_{2|\Delta v|/\delta v}^{\infty} dy \left[\frac{J_2(y)}{y}\right]^2 . \quad (16)$$

The scale of velocity change is

$$\delta v = \frac{2\hbar}{M_a b_m} , \quad (17)$$

which corresponds to diffractive scattering at the inelastic radius b_m. For dipole-dipole scattering, the line-broadening rate given by Eq. (68) determines b_m, while Eq. (79) determines b_m for dipole-quadrupole scattering. The kernels given by Eqs. (15) and (16) are normalized so that the integral over one-dimensional velocity changes Δv from $-\infty$ to ∞ gives the rate of transfer of coherence between transitions differing in magnetic quantum number by $\Delta M=1$ or $-1, \gamma_{|\Delta M|=1}$. For dipole-dipole or dipole-quadrupole collisions the respective rates are given by Eqs. (66) and (77).

Molecular constants for $^{12,13}CH_3F$ and CO_2 and $^{13}CH_3F$ line-broadening rates, are summaried in Table I. Using these parameters, coherence transfer rates, kernel $1/e$ widths, and maximum values $W(\Delta v=0)$ are calculated and summarized in Table II, where they are compared to experimental results. The error estimate for the measured kernel $1/e$ widths assumes that the velocity resolution is determined by $q\Delta v_{\rm RES}T \simeq 1$ or $\Delta v_{\rm res}=\lambda(2\pi T)$. Considering the simplicity of the approximations, the agreement is quite good, particularly for the kernel maximum values, which are measured directly in absolute units in the experiments.

Qualitatively, the shapes of the experimental kernels of Figs. 7 and 8 appear to be in good agreement with the

TABLE II. Measured and calculated collision parameters. (Calculated values in parentheses.)

Perturber	$\Delta v_{1/e}$ (cm/s)	$\gamma_{\Delta M}$ (MHz/Torr)	$W_{\Delta M}(0)$ [(kHz/Torr/(cm/s)]
$^{12}CH_3F$	230±60 (180)	3.1 (3.6)	8.9 (10.2)
CO_2	800±200 (570)	0.45 (0.46)	0.40 (0.36)

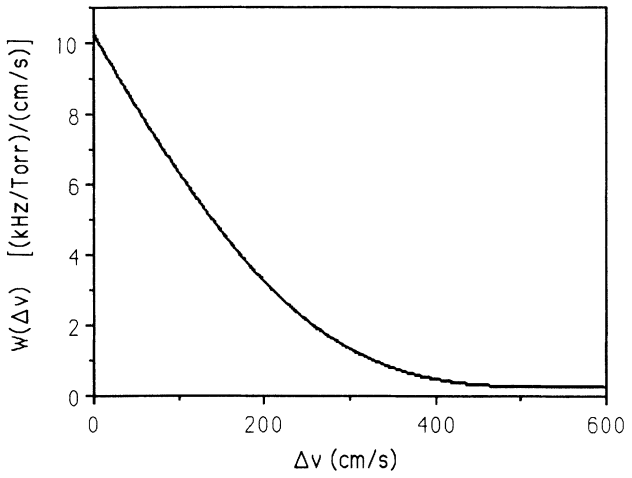

FIG. 10. Calculated dipole-dipole coherence-transfer kernel.

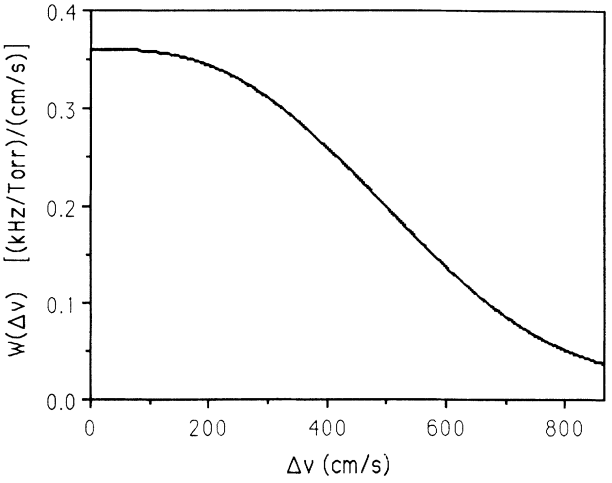

FIG. 11. Calculated dipole-quadrupole coherence-transfer kernel.

model kernels of Figs. 10 and 11. The dipole-quadrupole kernel seems to flatten near $\Delta v=0$, while the dipole-dipole kernel has a nonzero slope, i.e., the dipole-dipole kernel appears to have a cusp at $\Delta v=0$ as is normally expected for one-dimensional collision kernels.[21] The zero slope near $\Delta v=0$ can be traced back to the three-dimensional kernels. The dipole-quadrupole model three-dimensional kernel vanishes at $|\Delta\mathbf{v}|=0$. One expects this behavior since collisions which *change* the magnetic quantum numbers must be accompanied by a nonzero velocity change. Hence, all three-dimensional coherence-transfer kernels (with $\Delta M\neq 0$) should vanish at $|\Delta\mathbf{v}|=0$. This leads to a one-dimensional kernel with no cusp. For dipole-dipole collisions, the R^{-3} potential falls off so slowly that the corresponding model three-dimensional kernel does not vanish at the origin (it is finite). However, at very long range, retardation effects modify the R^{-3} force, leading to a faster roll off. Hence, one expects that in this case, if the correct dipole-dipole interaction were used, the corresponding three-dimensional kernel for $\Delta M=1$ coherence transfer also would vanish for sufficiently small $|\Delta\mathbf{v}|$. Then the one-dimensional kernel would have a zero slope at the origin. In the present experiments, the velocity resolution is not high enough to observe the exact behavior of the one-dimensional dipole-dipole kernel near the origin, since the measured velocity changes are already quite small. In this case, Eq. (15) is an adequate approximation. Hence, the agreement between the model and data kernels is reasonable.

The good agreement between the experimental and theoretical coherence-transfer rates, Table II, suggests that the assumption that the perturber does not inelastically scatter is approximately correct in this case. We examine this assumption by noting that if the active molecule states do not change J (as required for coherence transfer between transitions differing only in magnetic quantum number as studied here), energy conservation requires that

$$\tfrac{1}{2}\mu\mathbf{v}_r^2+E_p=\tfrac{1}{2}\mu\mathbf{v}'^2_r+E_{p'}\,, \tag{18}$$

where the prime denotes the initial state, E_p is the perturber internal energy, and v_r the relative speed. For small-angle scattering, $\mathbf{v}_r^2-\mathbf{v}'^2_r=(\mathbf{v}_r+\Delta\mathbf{v}_r)^2-\mathbf{v}'^2_r \simeq 2\mathbf{v}'_r\cdot\Delta\mathbf{v}_r$. The minimum $|\Delta\mathbf{v}_r|$ occurs for $\Delta\mathbf{v}_r$ parallel to $\mathbf{v}'_r$ and according to Eq. (18) is $|\Delta\mathbf{v}_r|=|E_{p'}-E_p|/(\mu v'_r)$. Hence, in the laboratory, the active molecule velocity change $\Delta\mathbf{v}=\mu\Delta\mathbf{v}_r/M_a$ must be greater than

$$|\Delta\mathbf{v}|>\frac{|E_p-E_{p'}|}{M_a v'_r} \tag{19}$$

for inelastic perturber scattering to occur. For CH_3F-CO_2 scattering, $|E_p-E_{p'}|\simeq 2\hbar cBJ_p$, where the CO_2 rotational constant $B\simeq 0.3$ cm^{-1} and $J_p\simeq 20$ at $T=293$ K. The relative speed $v'_r\simeq u_\mu=\sqrt{2kT/\mu}\simeq 5.0\times10^4$ cm/s, and the methyl fluoride mass is $M_a=35$ amu. In this case, $|\Delta\mathbf{v}|>828$ cm/s is required for perturber inelastic scattering. The coherence-transfer kernel for CH_3F-CO_2 scattering (Fig. 7) has a $1/e$ width near 800 cm/s. Hence, the perturbers will be scattered elastically over most of the kernel width. For CH_3F-CH_3F collisions, the smallest rotational constant $B\simeq 0.85$ cm^{-1} and $u_\mu\simeq 5.3\times10^4$ cm/s. In this case, $|\Delta\mathbf{v}|>2000$ cm/s for perturber inelastic scattering, so that the elastic assumption should be quite valid.

Finally, it is interesting to discuss the lack of coherence transfer for argon perturbers, which is expected to interact via a van der Waals potential. For a given state JKM, the rate for $JKM\rightarrow J'KM'$ collisions is proportional in lowest order to the square of the matrix element of the collision potential. Since we are interested in coherence transfer between state which *differ* in magnetic quantum number, only the rank two part of the van der Waals' potential is relevant. The scalar part cannot change M. In the framework of the isotropic approximation,[22] it is easy to show that the rate for a fixed final J' summed over all possible final M' is proportional to

$$P(J')=(2J'+1)\begin{pmatrix} J' & 2 & J \\ -K & 0 & K \end{pmatrix}^2 . \tag{20}$$

The $P(J')$ which are independent of the initial M obey the sum rule[23]

$$\sum_{J'} P(J')=1 . \tag{21}$$

From Eq. (21) the $P(J')$ may be interpreted as the probability for collisions which take the initial J to one final J' independent of final M'. Hence the probability of collisions which do not change J, as required for coherence transfer, is just $P(J'=J)$, where

$$P(J'=J)=\frac{[3K^2-J(J+1)]^2}{J(J+1)(2J-1)(2J+3)} . \tag{22}$$

This includes the possibility of $M'=M$ collisions and so overestimates the coherence-transfer probability slightly. For $J=4$, $K=3$, we find $P(J'=J)=\frac{7}{220}\simeq 0.03$. Hence, the coherence-transfer rate is at most 3% of the rate for J changing collisions in this system. Thus the echo signal decays exponentially due to inelastic collisions when argon is added, but the ratio of the echo signal with the Stark field on to that which the Stark field off, which measures coherence transfer, does not change appreciably.

V. PHASE DISRUPTION

Collision-induced infrared coherence transfer is particularly effective in infrared transitions when the inelastic (J changing, etc.) rates do not overwhelm the elastic M changing processes. In addition, it is necessary that the elastic phase shifts acquired by individual transitions not be large. A simple estimate of the collision-induced phase change $\Delta\varphi$ for impact parameters where coherence transfers occurs can be made as follows. The phase change which occurs for a particular $\Delta M=0$ transition $J_a,M\rightarrow J_b,M$ is approximately

$$|\Delta\varphi|=\left|\frac{1}{\hbar}\int_{-\infty}^{\infty}[V_b(M,M)-V_a(M,M)]dt\right| , \tag{23}$$

where $V=-\boldsymbol{\mu}\cdot\mathbf{E}_p(t)$, $\mathbf{E}_p(t)$ is the field of the perturber which interacts with the active molecule, and $V(M,M)$ is a diagonal matrix element. The integrated torque exerted on the molecule to reorient the radiator by one unit of angular momentum and transfer coherence is approximately such that

$$\left|\int_{-\infty}^{\infty} V_J(M,M\pm 1)dt\right|=\hbar , \tag{24}$$

where the off-diagonal matrix element of the potential for either J state is the order of the transition torque and we assume $J\simeq J_a\simeq J_b$ for large J. Equation (24) can be used to eliminate the field from Eq. (23). Assuming that all components of the perturber field are of equal magnitude on the average, the phase can be written in the form

$$|\Delta\varphi|=\left|\left[\frac{V_b(M,M)}{V_a(M,M)}-1\right]\frac{V_a(M,M)}{V_a(M,M,\pm 1)}\times\frac{1}{\hbar}\int_{-\infty}^{\infty}V_a(M,M\pm 1)dt\right| .$$

According to Eq. (24) with $J=J_a$ the integral factor is of order unity. Using the dipole matrix elements and the Wigner-Eckart theorem, we then have

$$|\Delta\varphi|=\left|\left[\frac{J_a(J_a+1)}{J_b(J_b+1)}-1\right]\frac{\begin{pmatrix} J_a & 1 & J_a \\ -M & 0 & M\end{pmatrix}}{\begin{pmatrix} J_a & 1 & J_a \\ -M & \mp 1 & M\pm 1\end{pmatrix}}\right| .$$

For low M where the off-diagonal matrix elements are largest, and coherence transfer most likely, the last factor is less than 1 and

$$|\Delta\varphi|<\left|\frac{J_a(J_a+1)}{J_b(J_b+1)}-1\right| . \tag{25}$$

For a high-J transition, the upper and lower states are shifted similarly and $|\Delta\varphi|\ll 1$, while for low J, significant phase shifts can occur, which destroy coherence. In our case, $J_a=4$, $J_b=5$, and $|\Delta\varphi|<\frac{1}{3}$. Hence, the phase shift is not very important.

VI. CONCLUSIONS

We have demonstrated that the technique of measuring the logarithm of two-pulse echo intensity versus Stark field permits study of the velocity change distributions (kernels) for coherence-transfer collisions. The method is based on the concept of compensating the Doppler shifts accompanying collision-induced velocity changes with the frequency shifts accompanying coherence M changes in the applied Stark field. The results of the measurements for the $\Delta M=1$ coherence-transfer rate and the kernel peak height at $\Delta v=0$, which differ by more than an order of magnitude between dipole-dipole and dipole-quadrupole potentials, are in good agreement with a simple theory which cuts off the impact parameter when inelastic collisions begin to occur. The calculated kernel $1/e$ widths are in reasonable agreement with the data considering the simplicity of the approximations made. The neglect of scalar van der Waals forces in the dipole-quadrupole case may not be quite justified.

The good agreement between the measurements and the simple theory shows that the tunable energy compensation technique yields reliable results. This suggests that the method, using either Stark or Zeeman fields, may be used to measure the shape of a variety of coherence-transfer collision kernels with much more detail than has been obtained in the present work.

ACKNOWLEDGMENTS

This research was supported by the National Science Foundation through Grant No. PHY-8703664.

APPENDIX: COHERENCE-TRANSFER VELOCITY-CHANGING KERNELS

In this section, we develop a general framework for calculating the average one-dimensional kernels which

are measured in the experiments. The kernels are then evaluated using a simplified model of the scattering amplitudes.

A. Kernel structure

The coherence-transfer process of interest is depicted in Fig. 1. Infrared coherence initially created on the transition b'-a' of frequency $\omega_{b'a'}$ is transferred to the transition b-a of frequency ω_{ba} in a collision with a perturber which changes internal state from $p' \rightarrow p$.

The three-dimensional kernel, which describes the arrival rate of coherence into the b-a transition accompanied by a velocity change of the active molecule $\mathbf{v}' \rightarrow \mathbf{v}$ is given by

$$W_{a \leftarrow a'}^{b \leftarrow b'}(\mathbf{v} \leftarrow \mathbf{v}') = 2N_p \sum_{p,p'} W_{\text{pert}}(E_{p'}) \int d\mathbf{v}_r \int d\mathbf{v}_r' W_{\text{pert}}(\mathbf{v}' - \mathbf{v}_r') \delta\left[\mathbf{v} - \mathbf{v}' - \frac{\mu}{M_a}(\mathbf{v}_r - \mathbf{v}_r')\right] \delta\left[v_r^2 - v_r'^2 + \frac{2(E_p - E_{p'})}{\mu}\right] \times f^*_{b \leftarrow b';p \leftarrow p'}(\mathbf{v}_r, \mathbf{v}_r') f_{a \leftarrow a';p \leftarrow p'}(\mathbf{v}_r, \mathbf{v}_r') \ . \tag{26}$$

In Eq. (26), f is a scattering amplitude, N_p the perturber density, W_{pert} are normalized Boltzmann distributions of the initial perturber internal state of energy $E_{p'}$ and velocity $\mathbf{v}_p' = \mathbf{v}' - \mathbf{v}_r'$. $\mathbf{v}, \mathbf{v}'$ are the final and initial active molecule velocities and $\mathbf{v}_r, \mathbf{v}_r'$ are the final and initial active molecule-perturber relative velocities. μ is the reduced mass and M_a is the active molecule mass. The δ functions conserve total momentum and energy. Note that for the problem at hand, the active molecule energy change for either the excited state $b' \rightarrow b$ or the ground state $a' \rightarrow a$ is negligible, since this transfer is between nearly degenerate (compared to the collision bandwidth) magnetic substates. For this reason, only the perturber energy change $E_p - E_{p'}$ appears in the energy-conserving δ function. Since the perturber bath is thermalized, an incoherent average over initial perturber states and a sum over final perturber states is employed for the kernel average.

One-dimensional kernels can be directly derived from Eq. (26) by averaging over a transverse distribution of active molecule initial velocities ($\mathbf{v}_\perp'$) and integrating over final transverse velocities ($\mathbf{v}_\perp$).[21] The resulting kernels are rather complicated, containing detailed information about the correlation between the velocity change along the laser field propagation direction and the magnetic state quantum numbers of the active molecule. For excitation with $\hat{\sigma}_+$ laser radiation propagating along the quantization axis ($\hat{\mathbf{z}}$), the cylindrical symmetry of the one-dimensional kernels ensures that the reorientation (ΔM) in the excited state $M_b - M_{b'}$ must be the same (for the cylindrical average) as that in the ground state ($M_a - M_{a'}$). However, with arbitrary laser polarizations in applied fields there is not always cylindrical symmetry.

It is well known that within the framework of the isotropic collision model for the decay *rates*, one can assume spherical symmetry.[22] The active molecule sees a more or less spherical distribution of perturbing molecule relative velocities, so long as the active molecules are excited near the center of the velocity distribution along the laser field propagation direction. Even with this approximation, the one-dimensional *kernels* generally will not have simple magnetic state behavior, because the measurement of the velocity change along a particular direction destroys the spherical symmetry. However, we expect that the departure from spherical symmetry will not be too large for the small-angle scattering which is of interest here. In order not to overload the derivation with details, we therefore impose spherical symmetry on the three-dimensional kernels by averaging first with a complete Maxwellian distribution $W_a(\mathbf{v}')$ of active molecule *initial* velocities holding the velocity change $\Delta\mathbf{v} = \mathbf{v} - \mathbf{v}'$ constant. Then, the resulting kernels are spherically averaged by integrating over solid angle $d\Omega_{\Delta\mathbf{v}}$ and dividing by 4π. In this way, an approximate isotropic three-dimensional kernel is obtained which has a simple structure and a velocity dependence only on $|\Delta\mathbf{v}|$. Integrated over $|\Delta\mathbf{v}|$, the kernel yields the usual isotropic model collision rates. The physical content of the three-dimensional kernels is then to relate the magnitude of the velocity change $|\Delta\mathbf{v}|$ to the coherence transfer between adjacent transitions differing in magnetic quantum number by ΔM in both the excited and ground states. One-dimensional kernels are then obtained by integrating over transverse components of $\Delta\mathbf{v}$.

With these approximations, the isotropic three-dimensional kernels obtained from Eq. (26) are given by

$$W_{a \leftarrow a'}^{b \leftarrow b'}(|\Delta\mathbf{v}|) \equiv \int \frac{d\Omega_{\Delta\mathbf{v}}}{4\pi} \int d\mathbf{v}' W_a(\mathbf{v}') W_{a \leftarrow a'}^{b \leftarrow b'}(\mathbf{v} \leftarrow \mathbf{v}')$$
$$= 2N_p \sum_{p,p'} W_{\text{pert}}(E_{p'}) \int d\mathbf{v}_r \int d\mathbf{v}_r' W_\mu(v_r') \times \frac{\delta(|\Delta\mathbf{v}| - \frac{\mu}{M_a}|\mathbf{v}_r - \mathbf{v}_r'|)}{4\pi|\Delta\mathbf{v}|^2} \delta\left[v_r^2 - v_r'^2 + \frac{2(E_p - E_{p'})}{\mu}\right] \times f^*_{b \leftarrow b';p \leftarrow p'}(\mathbf{v}_r \leftarrow \mathbf{v}_r') f_{a \leftarrow a';p \leftarrow p'}(\mathbf{v}_r \leftarrow \mathbf{v}_r') \ , \tag{27}$$

where $W_\mu(v_r')$ is a Maxwellian distribution of relative velocity, μ is the reduced mass, and M_a is the active molecule mass. Integrating Eq. (27) with $4\pi|\Delta\mathbf{v}|^2 d|\Delta\mathbf{v}|$ immediately gives the isotropic collision rates. Letting Δv be the velocity change along the laser field propagation direction, and ρ the magnitude of the perpendicular component of $\Delta\mathbf{v}$, we have

$$|\Delta\mathbf{v}| = \sqrt{\rho^2 + (\Delta v)^2} , \tag{28}$$

and the one-dimensional kernels are obtained by integrating over the transverse velocity changes as

$$W_{a\leftarrow a'}^{b\leftarrow b'}(\Delta v) = 2\pi \int_{|\Delta v|}^{\infty} d|\Delta\mathbf{v}|\, |\Delta\mathbf{v}|\, W_{a\leftarrow a'}^{b\leftarrow b'}(|\Delta\mathbf{v}|) , \tag{29}$$

where $\rho d\rho = |\Delta\mathbf{v}| d|\Delta\mathbf{v}|$ and at $\rho = 0$, $|\Delta\mathbf{v}| = |\Delta v|$.

In the following, we determine first the general structure of the isotropic kernels, Eq. (27), which turns out to be quite simple, as one would expect. Then, within the framework of a model, approximate scattering amplitudes are derived and one-dimensional kernels obtained.

Since we intend to use approximate WKB scattering amplitudes, we choose a collision frame as shown in Fig. 12. The collision frame is chosen so that the initial and final relative velocities $\mathbf{v}_r'$ and $\mathbf{v}_r$, respectively, lie in the $\hat{\mathbf{x}}'$-$\hat{\mathbf{z}}'$ plane. Hence, the polar angle θ of the $\hat{\mathbf{z}}' = \hat{\mathbf{v}}_r'$ axis with respect to the laboratory $\hat{\mathbf{z}}$ axis, and the azimuthal rotation φ of the $\hat{\mathbf{v}}_r'$ about the laboratory $\hat{\mathbf{z}}$ axis, determine two of the Euler angles of the collision frame. The rotation χ of the $\hat{\mathbf{x}}'$,$\hat{\mathbf{y}}'$ axes about the $\hat{\mathbf{z}}'$ axis, needed to bring $\hat{\mathbf{v}}_r$ into the $\hat{\mathbf{x}}'$-$\hat{\mathbf{z}}'$ plane, determines the final Euler angle. In the collision frame, the angle between the incoming and outgoing relative velocity is θ_c. The perturber-active molecule relative position is taken to be $\mathbf{R} = b\hat{\mathbf{b}} + z'\hat{\mathbf{z}}'$ in the collision frame, where $\hat{\mathbf{b}}$ is in the $\hat{\mathbf{x}}'$-$\hat{\mathbf{y}}'$ plane at an angle χ_c with respect to the $\hat{\mathbf{x}}'$ axis.

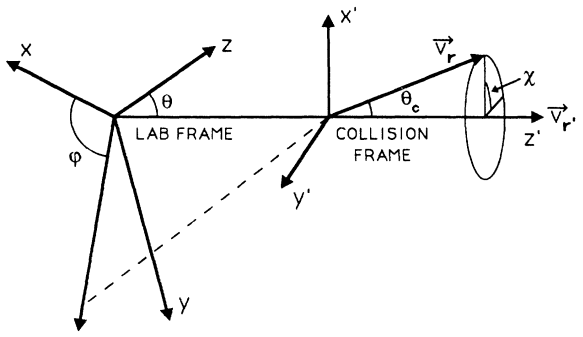

FIG. 12. Collision frame showing Euler angles.

There are a great many ways of representing the laboratory-frame scattering amplitudes in terms of collision frame matrix elements.[24] As we intend to perform simple lowest-order calculations for permanent multipole interactions, we expand the scattering operator f, which must be a scalar with respect to total angular momentum (active plus perturber plus relative orbital) in tensor operator form as

$$f = \sum_{l_1,q_1} T_{q_1}^{l_1}(a) U_{q_1}^{l_1 *}(p,\mathrm{rel}) , \tag{30}$$

where T operates on the active molecule (a) only and U operates on the perturber (p) and the relative motion (rel). Choosing a laboratory representation and taking matrix elements of Eq. (30) with respect to a *laboratory* angular momentum basis for the *active* molecule yields (using the Wigner-Eckart theorem for the active molecule operator T)

$$\langle a|f(p,\mathrm{rel})|a'\rangle = \sum_{l_1,q_1} (-1)^{J_a - m_a} \begin{pmatrix} J_a & l_1 & J_a \\ -m_a & q_1 & m_{a'} \end{pmatrix} \langle a\|T^{l_1}\|a'\rangle U_{q_1}^{l_1 *}(p,\mathrm{rel}) , \tag{31}$$

where J_a, m_a, J_a, and $m_{a'}$ are angular momentum and laboratory-frame magnetic quantum numbers for the active molecule state $a(a')$.

Although we have chosen a laboratory representation for the T and U operators, the matrix elements for the relative motion contained in U are most easily evaluated using the corresponding collision frame operators. The laboratory frame (q_1) and collision frame (q_1')U operators are related according to[23]

$$U_{q_1}^{l_1} = \sum_{q_1'} U_{q_1'}^{l_1} \mathcal{D}_{q_1' q_1}^{(l_1)}(\mathcal{R}) , \tag{32}$$

where $\mathcal{R} \equiv \chi,\theta,\phi$ are the Euler angles of the collision frame with respect to the laboratory frame. Combining Eqs. (30)–(32) yields the matrix of f in the form

$$\langle ap\|f(\mathbf{v}_r,\mathbf{v}_r')|a'p'\rangle = \sum_{l_1,q_1} (-1)^{J_a - m_a} \begin{pmatrix} J_a & l_1 & J_a \\ -m_a & q_1 & m_{a'} \end{pmatrix} \mathcal{D}_{q_1 q_1}^{l_1 *}(\mathcal{R}) \langle ap\|f_{q_1'}^{l_1}(\mathbf{v}_r,\mathbf{v}_r')\|ap\rangle , \tag{33}$$

where

$$\langle ap\|f_{q_1'}^{l_1}(\mathbf{v}_r,\mathbf{v}_r')\|ap\rangle \equiv \langle a\|T^{l_1}\|a'\rangle \langle p|U_{q_1'}^{l_1 *}(\mathbf{v}_r,\mathbf{v}_r')|p'\rangle . \tag{34}$$

Note that the matrix of $f_{q_1'}^{l_1}$ in Eq. (33) is reduced (double bar) with respect to the *active* molecule states only. The form of Eq. (33) is still quite general.

The integrations over $\mathbf{v}_r,\mathbf{v}_r'$ required to evaluate the

kernel 27 can be carried out using

$$d^3\mathbf{v}_r = dv_r v_r^2 (\sin\theta_c) d\theta_c d\chi \ , \qquad d^3\mathbf{v}_r' = dv_r' v_r'^2 (\sin\theta) d\theta\, d\varphi \ , \tag{35}$$

where the $\mathbf{v}_r$ integration is done to a frame rotated so that $\hat{\mathbf{z}}''=\hat{\mathbf{v}}_r'$. This frame differs from the collision frame by the azimuthal rotation χ about $\hat{\mathbf{z}}''=\hat{\mathbf{z}}'=\mathbf{v}_r'$ needed to bring $\mathbf{v}_r$ into the $\hat{\mathbf{x}}'$-$\hat{\mathbf{z}}'$ plane of Fig. 12. With this choice of angles,

$$|\mathbf{v}_r-\mathbf{v}_r'| = (v_r^2+v_r'^2-2v_r v_r'\cos\theta_c)^{1/2} \ . \tag{36}$$

The matrix of $f_{q_1'}^{l_1'}(\mathbf{v}_r,\mathbf{v}_r')$ depends only on the angle θ_c since $\mathbf{v}_r$ and $\mathbf{v}_r'$ always lie in the $\hat{\mathbf{x}}'$-$\hat{\mathbf{z}}'$ plane in the collision frame. Using $\mathcal{R}\equiv\chi,\theta,\varphi$ and $d\mathcal{R}\equiv\sin\theta\, d\theta\, d\varphi\, d\chi$, the matrices of the rotation operator obey the orthogonality relationship[23]

$$\int d\mathcal{R}\, \mathcal{D}^{l_1'}_{q_1'q_1}(\mathcal{R})\mathcal{D}^{l_2*}_{q_2'q_2}(\mathcal{R}) = \frac{8\pi^2}{2l_1+1}\delta_{l_2'l_1}\delta_{q_2q_1}\delta_{q_2'q_1'} \ . \tag{37}$$

Equations (27), (33) and (37) yield the three-dimensional kernels in the following form:

$$\begin{aligned} W_{a\leftarrow a'}^{b\leftarrow b'}(|\Delta\mathbf{v}|) = 2N_p \sum_{pp'} W_{\text{pert}}(E_{p'}) \int_0^\infty dv_r' v_r'^2 W_\mu(v_r') \\ \times \int_0^\infty dv_r v_r^2 \delta\left[v_r^2 - v_r'^2 + \frac{2(E_p-E_{p'})}{\mu} \right] \\ \times \int_0^\pi d\theta_c \sin\theta_c \frac{\delta[|\Delta\mathbf{v}|-(\mu/M_a)(v_r^2+v_r'^2-2v_r v_r'\cos\theta_c)^{1/2}]}{4\pi|\Delta\mathbf{v}|^2} \\ \times \sum_{l_1 q_1} (-1)^{J_2-m_2+J_b-m_b} \begin{pmatrix} J_a & l_1 & J_a \\ -m_a & q_1 & m_{a'} \end{pmatrix} \begin{pmatrix} J_b & l_1 & J_b \\ -m_b & q_1 & m_{b'} \end{pmatrix} \\ \times \frac{8\pi^2}{2l_1+1} \sum_{q_1'} \langle bp \| f_{q_1'}^{l_1'}(v_r,v_r',\theta_c) \| bp' \rangle^* \langle ap \| f_{q_1'}^{l_1'}(v_r,v_r',\theta_c) \| ap' \rangle \ . \end{aligned} \tag{38}$$

In the small-angle ($\theta_c \ll 1$) long-range scattering limit, $\sin\theta_c \simeq \theta_c$ and $2(E_p-E_{p'}) \ll v_r'^2$. For this case, the kernel reduces to

$$W_{a\leftarrow a'}^{b\leftarrow bl'}(|\Delta\mathbf{v}|) = \int_0^\infty dv_r' 4\pi v_r'^2 W_\mu(v_r') W_{a\leftarrow a'}^{b\leftarrow b'}(|\Delta\mathbf{v}|,v_r') \equiv \langle W_{a\leftarrow a'}^{b\leftarrow b'}(|\Delta\mathbf{v}|,v_r') \rangle \ , \tag{39}$$

where

$$\begin{aligned} W_{a\leftarrow a'}^{b\leftarrow b'}(|\Delta\mathbf{v}|,v_r') = N_p v_r' \left[\frac{M_a}{\mu v_r'} \right]^2 \frac{1}{2|\Delta\mathbf{v}|} \sum_{pp'} W_{\text{pert}}(E_{p'}) \sum_{l_1,q_1} \frac{(-1)^{J_a-m_a+J_b-m_b}}{2l_1+1} \begin{pmatrix} J_a & l_1 & J_a \\ -m_a & q_1 & m_{a'} \end{pmatrix} \begin{pmatrix} J_b & l_1 & J_b \\ -m_b & q_1 & m_{b'} \end{pmatrix} \\ \times \sum_{q_1'} \langle bp \| f_{q_1'}^{l_1'}(v_r,v_r',\theta_c) \| bp' \rangle^* \langle ap \| f_{q_1'}^{l_1'}(v_r,v_r',\theta_c) \| ap' \rangle \end{aligned} \tag{40}$$

and

$$\theta_c \simeq \left[\left[\frac{M_a|\Delta\mathbf{v}|}{\mu v_r'} \right]^2 - \left[\frac{E_p-E_{p'}}{\mu v_r'^2} \right]^2 \right]^{1/2} , \tag{41}$$

and $v_r \simeq v_r' - (E_p-E_{p'})/(\mu v_r')$ in $f_{q_1'}^{l_1'}$. Note that for nonzero contributions to the kernel with $E_p-E_{p'}\neq 0$, the minimum $|\Delta\mathbf{v}|$ required by energy and momentum conservation is $|E_p-E_{p'}|/(M_a v_r')$, according to Eq. (41), in agreement with Eq. (19).

B. Scattering amplitudes

Generally, the scattering amplitudes can always be written in the form[25]

$$\langle ap | f(\mathbf{v}_r,\mathbf{v}_r') | a'p' \rangle = -\frac{\mu V_0}{2\pi\hbar^2} \langle \mathbf{v}_r ap | \hat{\mathbf{V}} | \Psi^{(+)}_{\mathbf{v}_r' a'p'} \rangle \ , \tag{42}$$

where V_0 is the quantization volume, $\hat{\mathbf{V}}$ the collision potential, and $\Psi^{(+)}$ the scattering state which reduces to the incoming active-perturber internal-relative motion state at large distance prior to the scattering region, where $\hat{\mathbf{V}}$ is zero. The final state $|\mathbf{v}_r ap\rangle$ is given by (box normalization)

$$\langle \mathbf{R} | \mathbf{v}_r ap \rangle = \frac{e^{i\mathbf{k}\cdot\mathbf{R}}}{\sqrt{V_0}} |a\rangle |p\rangle \ , \tag{43}$$

where $\hbar\mathbf{k}=\mu\mathbf{v}_r$ and $\mathbf{R}$ is the active molecule-perturber relative separation.

The scattering state can be represented in the form (with $\hbar\mathbf{k}'=\mu\mathbf{v}_r'$)

$$\langle \mathbf{R}|\Psi^{(+)}_{\mathbf{v}_r'a'p'}\rangle=\frac{e^{i\mathbf{k}'\cdot\mathbf{R}}}{\sqrt{V_0}}\hat{\mathbf{F}}(\mathbf{R})|a'\rangle|p'\rangle\ , \tag{44}$$

where $\hat{\mathbf{F}}(\mathbf{R})$ is an operator on the active molecule and perturber internal states (a',p') which tends to the identity operator $\hat{\mathbf{I}}$ at large relative distance $|\mathbf{R}|$. Equations (42)–(44) yield the scattering amplitudes in the form

$$\langle ap|f(\mathbf{v}_r,\mathbf{v}_r')|a'p'\rangle$$
$$=-\frac{\mu}{2\pi\hbar^2}\int d^3\mathbf{R}\,e^{i(\mathbf{k}'-\mathbf{k})\cdot\mathbf{R}}\langle ap|\hat{\mathbf{V}}\hat{\mathbf{F}}|a'p'\rangle\ . \tag{45}$$

By using the WKB approximation in the collision frame with $\mathbf{R}=\mathbf{b}+z\hat{\mathbf{z}}'$ (Fig. 12), it is straightforward to substitute Eq. (44) into the Schrödinger equation and to obtain a formal expression for the position-dependent operator $\hat{\mathbf{F}}(\mathbf{R})$ and hence for the scattering amplitudes. Then the tensorial components of the scattering amplitudes with respect to the active molecule internal states can be determined by comparing with the analog of Eq. (30) in the collision frame. This determines $U^{l}_{q_1'}{}^{*}$ and hence the matrix elements given by Eq. (34). For the purpose of this paper, we consider a simple approximation instead of calculating the exact structure of the $\hat{\mathbf{F}}$ operator, since our interest is, from the outset, in lowest-order results.

The coherence-transfer process which is of interest here requires that coherence between the two states (a',b') of Fig. 1 survive to a significant extent the transfer to some neighboring transition (a,b). For the case where the states (a',b') have the same magnetic quantum number M' and (a,b) the magnetic quantum number M, this process corresponds to a tipping of the radiator by $\Delta M=M-M'$. One expects that for sufficiently close encounters between active and perturber molecules, J changing collisions will occur with high probability and the optical coherence of the active molecule will be destroyed. Since for molecules with permanent moments J changes will occur at quite long range, one expects that coherence transfer in such systems also must occur predominantly at long range, accompanied by very small velocity changes. This will be true provided that the scalar potential (e.g., scalar van der Waals) which preserves rotational states, does not extend significantly outside the destruction radius. Further, for vibrational (infrared) transitions in the high-J limit, one expects similar collision potentials and little dephasing.[17]

Based on these ideas, we consider the following approximation for small velocity changes.

(i) Inside some minimum radius b_m, the $\hat{\mathbf{F}}$ operator can be considered to vanish for any input state and further can be taken as a scalar. The radius b_m is derived from the known destruction (broadening) cross section, assumed due to predominantly J-changing collisions.[26] This is equivalent to introducing complex partial wave phase shifts for which the imaginary part (destruction) is large for $b<b_m$, and negligible for $b>b_m$. Note that our treatment is reasonable only for $\Delta M\neq 0$ collisions since we neglect elastic shadow scattering which arises from the absorbing region, $b<b_m$, when we set $\hat{F}=0$. As our experiment studies only coherence *transfer* with $\Delta M\neq 0$, as described above, this approximation is acceptable. Admittedly, the coherence transfer and J-changing processes probably occur at quite similar ranges for permanent multipole interactions, so that the abrupt cutoff approximation for impact parameters below b_m is not expected to be very accurate. Nevertheless, we use it anyway in order to obtain a simple treatment and demonstrate that the experiments yield reasonable results.

(ii) We consider velocity changes $|\Delta\mathbf{v}|$ smaller than the threshold $|E_p-E_{p'}|/(M_a v_r')$ for inelastic perturber scattering [see Eq. (41)]. In this case, the perturber rotational quantum numbers J_p and K_p do not change. This is justified above, using the magnitude of the active molecule velocity changes measured in the experiments. Note that for the coherence-transfer process measured in the present experiments, only the *magnetic* states of the active molecule change and $E_a-E_{a'}=0$, as discussed above.

(iii) We assume that the dominant M-changing collision potential $\hat{\mathbf{V}}$ is the lowest-order permanent multipole interaction.

(iv) We consider symmetric top and linear molecules only.

The permanent multipole interaction $\hat{\mathbf{V}}$ is written in the form[23]

$$\hat{\mathbf{V}}(\mathbf{R})=\sum_{l_1,l_2,m_1,m_2,m} q^{(a)}_{l_1m_1}q^{(p)}_{l_2m_2}X^{l_1+l_2}_{m}(\mathbf{R})\times\begin{pmatrix} l_1 & l_2 & l_1+l_2\\ m_1 & m_2 & m\end{pmatrix}, \tag{46}$$

where

$$q^{(i)}_{lm}\equiv\left[\frac{4\pi}{2l+1}\right]^{1/2}\int d\mathbf{x}'r'^{l}Y_{lm}(\theta',\varphi')\rho_i(\mathbf{x}') \tag{47}$$

are the active molecule $(i=a)$ or perturber $(i=p)$ permanent multipole operators, and the relative motion operator is given by

$$X^{l_1+l_2}_{m}(\mathbf{R})=(-1)^{l_1}\left[\frac{[2(l_1+l_2)]!4\pi}{(2l_1)!(2l_2)!}\right]^{1/2}\frac{R^{l}Y_{lm}(\hat{\mathbf{R}})}{R^{2l+1}}\ , \tag{48}$$

where $l=l_1+l_2$ in Eq. (48). $R^{l}Y_{lm}$ is a solid harmonic which can be written in terms of Cartesian components of $\mathbf{R}$.[23]

Using Eqs. (30), (45), and (46) we identify $T^{l_1}_{q_1}(a)$ with $q^{(a)}_{l_1m_1}$ (i.e., $q_1=m_1$). Hence,

$$\langle a\|T^{l_1}\|a'\rangle=\langle a\|q^{(a)}_{l_1}\|a'\rangle\ . \tag{49}$$

Further, for $\hat{\mathbf{F}}$ scalar,

$$U_{q_1}^{l_1*}(p:\mathbf{R})=-\frac{\mu V_0}{2\pi\hbar^2}\sum_{l_2,m_2,m} q_{l_2 m_2}^{(p)} X_m^{l_1+l_2}(\mathbf{R}) \begin{bmatrix} l_1 & l_2 & L_1+l_2 \\ q_1 & m_2 & m \end{bmatrix} \hat{\mathbf{F}}(\mathbf{R}) . \tag{50}$$

The reduced scattering amplitudes, Eq. (34), are then given by

$$\langle ap\|f_{q_1'}^{l_1}(\mathbf{v}_r,\mathbf{v}_r')\|a'p'\rangle=-\frac{\mu}{2\pi\hbar^2}\langle a\|q_{l_1}^{(a)}\|a'\rangle \sum_{l_2,m_2',m'} \langle p|Q_{l_2 m_2'}^{(p)}|p'\rangle \begin{bmatrix} l_1 & l_2 & l_1+l_2 \\ q_1' & m_2' & m' \end{bmatrix} S_{m'}^{l_1+l_2}(\theta_c) , \tag{51}$$

where the matrix element is reduced only with respect to the *active* molecule internal states and

$$S_{m'}^{l_1+l_2}(\theta_c)=\int d^3\mathbf{R}\, F(\mathbf{R}) e^{i(\mathbf{k}'-\mathbf{k})\cdot\mathbf{R}} X_{m'}^{l_1+l_2}(\mathbf{R}) . \tag{52}$$

All magnetic quantum numbers (q_1',m_2',m') are referred to the collision frame.

Using $\mathbf{R}=b\hat{\mathbf{b}}+z\hat{\mathbf{z}}'$ for the relative position in the collision frame, Fig. 12 shows that $(\mathbf{k}'-\mathbf{k})\cdot\mathbf{R}\simeq -k'b\theta_c\cos\chi_c$, for $\theta_c\ll 1$.[27] The F operator is taken as $F(\mathbf{R})=0$ for $b<b_m$ and 1 otherwise. With $d\mathbf{R}=b\,db\,d\chi_c dz$, Eq. (52) takes the form

$$S_{m'}^{l_1+l_2}(\theta_c)=(-1)^{m'}\int_{b_m}^{\infty} b\,db\,J_{m'}(k'b\theta_c) \times\int_{-\infty}^{\infty} dz\, X_{m'}^{l_1+l_2}(b,z,\chi_c=0) , \tag{53}$$

where $J_{m'}$ is a Bessel function of order m',[28]

$$J_{m'}(k'b\theta_c)=(-i)^{m'}\int_0^{2\pi} d\chi_c \frac{1}{2\pi} e^{ik'b\theta_c\cos\chi_c+im'\chi_c} , \tag{54}$$

and[28]

$$J_{-m'}(x)=(-1)^{m'}J_{m'}(x)=J_{m'}(-x) . \tag{55}$$

The three-dimensional kernels, Eq. (40), are now evaluated using the symmetric top angular momentum states:

$$\begin{aligned} |a\rangle &\equiv |J_a K_a m_a\rangle , \\ |a'\rangle &\equiv |J_a K_a m_{a'}\rangle , \\ |p\rangle &\equiv |J_p K_p m_p\rangle , \\ |p'\rangle &\equiv |J_p K_p m_{p'}\rangle , \end{aligned} \tag{56}$$

where J is the rotational quantum number and K the projection on the molecular symmetry axis. Note that we assume that the perturber scatters without changing internal energy $(J_p=J_{p'},\ K_p=K_{p'})$ for the small velocity changes of interest here, as discussed above. Since the perturber states are isotropically distributed and appear in the kernel as $|p\rangle\langle p|$ and $|p'\rangle\langle p'|$, the sums over magnetic states in the collision kernel are straightforwardly carried out using the Wigner-Eckart theorem and $3j$ symbol sum rules to obtain

$$\begin{aligned} &W_{m_a\leftarrow m_{a'};m_b\leftarrow m_{b'}}^{J_a K_a;J_b K_b}(|\Delta\mathbf{v}|,v_r') \\ &=\sum_{l_1,q_1}(-1)^{J_b-m_b+J_a-m_a}\sqrt{(2J_b+1)(2J_a+1)} \begin{bmatrix} J_b & l_1 & J_b \\ -m_b & q_1 & m_{b'} \end{bmatrix} \begin{bmatrix} J_a & l_1 & J_a \\ -m_a & q_1 & m_{a'} \end{bmatrix} \\ &\times(-1)^{J_b-K_b+J_a-K_a}\sqrt{(2J_b+1)(2J_a+1)} \begin{bmatrix} J_b & l_1 & J_b \\ -K_b & 0 & K_b \end{bmatrix} \begin{bmatrix} J_a & l_1 & J_a \\ -K_a & 0 & K_a \end{bmatrix} \sum_{l_2} W_{l_1 l_2}(|\Delta\mathbf{v}|,v_r') , \end{aligned} \tag{57}$$

where

$$W_{l_1 l_2}(|\Delta\mathbf{v}|,v_r')=N_p\eta(l_2)\frac{(M_a/\hbar^2)^2}{2v_r'|\Delta\mathbf{v}|}\frac{|q_{l_1 0}^{(a)}|^2}{2l_1+1}\frac{|q_{l_2 0}^{(p)}|^2}{2l_2+1}\sum_{q'}\frac{|S_{q'}^{l_1+l_2}(M_a|\Delta\mathbf{v}|/\mu v_r')|^2}{2(l_1+l_2)+1} . \tag{58}$$

The small vibrational change in the permanent moments between the a and b states has been neglected in Eq. (58). The active and perturber permanent multipole moments (referred to the molecule symmetry axis) are $q_{l_1 0}^{(a)}$ and $q_{l_2 0}^{(p)}$, respectively. $S_{q'}^{l_1+l_2}(\theta_c)$ is given by Eq. (53) and

$$\eta(l_2)=\sum_{J_{p'},K_p}(2J_{p'}+1)\frac{e^{-E_{J_{p'},K_p}/k_B T}}{Z_p} \times \begin{bmatrix} J_{p'} & l_2 & J_{p'} \\ -K_p & 0 & K_p \end{bmatrix}^2 . \tag{59}$$

The η-function averages the perturber multipole moment over $J_{p'}$ and K_p, the projection of $\mathbf{J}_p$ on the perturber symmetry axis. Z_p is the perturber partition function. It is assumed that $\Delta J_p=0$, as discussed above, for long-range coherence-preserving collisions.

For the Stark tunable energy compensation experiments with $\hat{\mathbf{z}}$-polarized laser and Stark fields, we have $m_{a'}=m_{b'}=M'$ and $m_a=m_b=M$. Further, for the $v_3=0\rightarrow 1$ transition of $^{13}CH_3F$, $K_a=K_b=K$. In the high-J limit, $J\gg l_1$, which was assumed in order to obtain the simple relationship between the echo intensity versus Stark field and the coherence-transfer kernels, we can take

$$J\simeq\frac{J_a+J_b}{2}\simeq J_a\simeq J_b\gg l_1 \ . \tag{60}$$

For a given $M-M'\equiv\Delta M$, only terms in Eq. (57) with $q_1=\Delta M$ contribute to the kernel. In this case, initial M' averaged kernels are obtained with the approximation

$$(-1)^{J_b-M+J_a-M}\sqrt{(2J_a+1)(2J_b+1)}\begin{pmatrix} J_b & l_1 & J_b \\ -M & \Delta M & M'\end{pmatrix}\begin{pmatrix} J_a & l_1 & J_a \\ -M & \Delta M & M'\end{pmatrix}$$
$$\simeq\frac{1}{2J+1}\sum_{M'}(2J+1)\begin{pmatrix} J & l_1 & J \\ -M & \Delta M & M'\end{pmatrix}=\frac{\Theta(l_1-|\Delta M|)}{2l_1+1} \ , \tag{61}$$

where the step function $\Theta(x)=1$ for $x\geq 0$ and is zero otherwise. The initial M' averaged kernels for $|\Delta M|>0$ then take the simplified form [with J given by Eq. (60)]

$$W^J_{\Delta M}(|\Delta\mathbf{v}|,v_r')=\sum_{l_1}\frac{\Theta(l_1-|\Delta M|)}{2l_1+1}(2J+1)\begin{pmatrix} J & l_1 & J \\ -K & 0 & K\end{pmatrix}^2\sum_{l_2}W_{l_1l_2}(|\Delta\mathbf{v}|,v_r') \ , \tag{62}$$

which is symmetric in ΔM due to the initial M' averaging. In this approximation, infrared coherence-transfer kernels are identical to state population transfer kernels, for magnetic quantum number changing collisions. This assumption has been used previously in studies of elastic velocity changing collisions, where it was assumed that the ground- and excited-state scattering amplitudes for infrared transitions were nearly identical, so that the kernel could be taken as real (the phase change is neglected).[17] Note that Eq. (62) is valid only for coherence *transfer* ($\Delta M\neq 0$), as discussed above, since elastic shadow scattering is neglected.

For later use, the integral of Eq. (62) over $|\Delta\mathbf{v}|$ yields the coherence-transfer rate for $\Delta M\neq 0$ collisions

$$\gamma^J_{\Delta M}=\int_0^\infty 4\pi d|\Delta\mathbf{v}||\Delta\mathbf{v}|^2\langle W^J_{\Delta M}(|\Delta\mathbf{v}|,v_r')\rangle \ , \tag{63}$$

where the average over initial relative velocity v_r' according to Eq. (39) is denoted by $\langle\ \rangle$.

C. Permanent multipole coherence-transfer kernels

1. Dipole-dipole scattering

The simplest permanent moment interaction is the dipole-dipole potential which dominates for symmetric top active and perturber molecules with large permanent dipole moments along the symmetry axis. For this case, $l_1=l_2=1$ and the kernel in Eq. (58) takes the form

$$W_{11}(|\Delta\mathbf{v}|,v_r')=N_p\eta(1)\frac{(M_a/\hbar^2)^2}{2v_r'|\Delta\mathbf{v}|}\frac{|\mu_0^{(a)}|^2}{3}\frac{|\mu_0^{(p)}|^2}{3}\frac{2|S_2^{1+1}(M_a|\Delta\mathbf{v}|/\mu v_r')|^2}{5} \ , \tag{64}$$

where $\mu_0^{(a)}$ is the active molecule permanent dipole moment and $\mu_0^{(p)}$ that of the perturber. The z integrals in the S functions of Eq. (53) vanish except for $q'=\pm 2$. With $k=k'=\mu v_r'/\hbar$,

$$S^{1+1}_{\pm 2}(\theta_c)=-2\sqrt{5}\int_{b_m}^\infty db\frac{1}{b}J_2(kb\theta_c)$$
$$=-2\sqrt{5}\frac{J_1(kb_m\theta_c)}{kb_m\theta_c} \ . \tag{65}$$

It is interesting to note that according to Eq. (53), for $m'\neq 0$, $S^{l_1+l_2}_{m'}(\theta_c=0)\rightarrow 0$, provided that the integrand vanishes sufficiently fast as $b\rightarrow\infty$, as it does for the dipole-quadrupole interaction discussed below. This is reasonable, since for $\Delta M\neq 0$ collisions, one expects that if $|\Delta\mathbf{v}|=0$ (no active molecule velocity change) which implies $|\Delta\mathbf{v}_r|=0$, there can be no change in the magnetic quantum numbers. For the dipole-dipole interaction, we find that the b integrand vanishes too slowly, leading to

peak at $\theta_c=0$. In reality, however, one expects that the dipole-dipole potential ($\propto R^{-3}$) is altered at long range by retardation effects and vanishes faster than R^{-3}, so that for small θ_c, $S(\theta_c)\rightarrow 0$, as it should. For the present, we will neglect this more exact behavior, since for the velocity resolution attainable in our experiment, the one-dimensional kernels which are derived using Eq. (65) adequately model the data. With this approximation, the $\Delta M=1$ coherence-transfer rate averaged over v_r' is obtained by direct integration of Eq. (63) in the form

$$\gamma_{\Delta M=1}^{d-d}\equiv N_p u_\mu \pi \frac{b_0^4}{b_m^2} , \tag{66}$$

where $u_\mu=\sqrt{2k_BT/\mu}$, with μ the reduced mass and

$$b_0^4\equiv\frac{8}{9}\frac{K^2}{3J(J+1)}\eta(1)\frac{|\mu_0^{(a)}|^2|\mu_0^{(p)}|^2}{(\hbar u_\mu)^2} . \tag{67}$$

The destruction radius b_m is determined from the line-broadening rate γ_B. Since an abrupt cutoff is used in the scattering amplitude impact parameter integration, for consistency, an abrupt cutoff is used to determine the destruction radius from the line-broadening rate. Hence, the destruction cross section is taken as πb_m^2. Then

$$\gamma_B=N_p\langle v_r\rangle\pi b_m^2=N_p u_\mu\frac{2}{\sqrt{\pi}}\pi b_m^2 . \tag{68}$$

In Eq. (68), we neglect the dependence of b_m on the relative speed, which has little effect on the accuracy. A more accurate treatment would allow a probability of destruction $P(b)$ for each impact parameter[22] in the destruction cross section and a corresponding factor in the impact parameter integration for the scattering amplitudes. However, the three-dimensional kernels would not be obtainable in closed form. Finally, assuming that the perturber internal energy does not change for the small velocity changes of interest here, Eq. (59) yields

$$\eta(1)=\left\langle\frac{K_p^2}{J_p(J_p+1)}\right\rangle =\frac{1}{Z_p}\sum_{J_pK_p} e^{-E_{J_pK_p}/k_BT}(2J_p+1)\frac{K_p^2}{J_p(J_p+1)} , \tag{69}$$

where

$$E_{J_pK_p}=BJ_p(J_p+1)+(A-B)K_p^2 . \tag{70}$$

For CH_3F perturbers, $\eta(1)=0.138$. Using the rate given by Eq. (66), the three-dimensional kernel takes the form

$$W_{\Delta M=1}^{d-d}(|\Delta\mathbf{v}|)=\gamma_{\Delta M=1}^{d-d}\frac{2}{\pi(\delta v)^2|\Delta\mathbf{v}|}\left|\frac{J_1(2|\Delta\mathbf{v}|/\delta v)}{(2|\Delta\mathbf{v}|/\delta v)}\right|^2 , \tag{71}$$

where

$$\delta v\equiv\frac{2\hbar}{M_a b_m} . \tag{72}$$

The weak dependence of δv on the relative speed v_r' is neglected so that the integral of Eq. (71) over $|\Delta\mathbf{v}|$ according to Eq. (63) yields the rate $\gamma_{\Delta M=1}^{d-d}$ given by Eq. (66).

The one-dimensional kernel obtained according to Eq. (29) from the three-dimensional kernel of Eq. (71) is given by

$$W_{\Delta M=1}^{d-d}(\Delta v)=\gamma_{\Delta M=1}^{d-d}\frac{2}{\delta v}\int_{2|\Delta v|/\delta v}^{\infty}dy\left[\frac{J_1(y)}{y}\right]^2 , \tag{73}$$

where Δv is the component of the velocity change along the laser field propagation direction. From this, the value of the kernel for $\Delta v=0$ is readily obtained, as is the kernel $1/e$ width. One finds $\Delta v_{1/e}=0.6\delta v$.

2. *Dipole-quadrupole scattering*

For dipole-quadrupole scattering, $l_1=1$, $l_2=2$, and $q_{10}^{(a)}=\mu_0^{(a)}$, $q_{20}^{(p)}=Q_{zz}/2$, where

$$Q_{zz}=\int d\mathbf{r}'\rho(\mathbf{r}')(3z'^2-r'^2) \tag{74}$$

is the perturber permanent quadrupole moment. In this case, Eq. (58) takes the form

$$W_{12}(|\Delta\mathbf{v}|,v_r')=N_p\eta(2)\frac{(M_a/\hbar^2)^2}{2v_r'|\Delta\mathbf{v}|}\frac{|\mu_0^{(a)}|^2}{3}\frac{|Q_{zz}^{(p)}|^2}{20}\frac{2|S_3^{1+2}(M_a|\Delta\mathbf{v}|/\mu v_r')|^2}{7} . \tag{75}$$

The z integrals in the S functions of Eq. (53) vanish except for $q'=\pm 3$, where

$$S_{\pm 3}^{1+2}(\theta_c)=\left[\frac{7\times 16}{3}\right]^{1/2}\int_{b_m}^{\infty}db\frac{1}{b^2}J_3(kb\theta_c) =\left[\frac{7\times 16}{3}\right]^{1/2}\frac{J_2(kb_m\theta_c)}{kb_m\theta_c} . \tag{76}$$

The v_r' averaged rate for $\Delta M=1$ coherence transfer is obtained from Eq. (63) as

$$\gamma_{\Delta M=1}^{d-Q}\equiv N_p u_\mu\left\langle\left[\frac{v_r'}{u_\mu}\right]^{1/3}\right\rangle\pi\frac{b_0^6}{b_m^4} , \tag{77}$$

where the factor in the angular brackets is 1.02 and

$$b_0^6\equiv\frac{4}{45}\frac{K^2}{3J(J+1)}\eta(2)\frac{|\mu_0^{(a)}|^2|Q_{zz}^{(p)}|^2}{(\hbar u_\mu)^2} , \tag{78}$$

with $\eta(2)$ given by Eq. (59) for $l_2=2$. For CO_2, $K_p=0$

and $\eta(2)=0.25$. The destruction radius is determined using Eq. (68), which assumes an abrupt cutoff radius:

$$\gamma_B = N_p u_\mu \frac{2}{\sqrt{\pi}} \pi b_m^2 \ . \tag{79}$$

Using the rate given by Eq. (77), the three-dimensional kernel takes the form

$$W^{d-Q}_{\Delta M=1}(|\Delta \mathbf{v}|) = \gamma^{d-Q}_{\Delta M=1} \frac{4}{\pi(\delta v)^2 |\Delta \mathbf{v}|} \left| \frac{J_2(2|\Delta \mathbf{v}|/\delta v)}{(2|\Delta \mathbf{v}|/\delta v)} \right|^2 , \tag{80}$$

where δv takes the form of Eq. (72) and b_m is determined by Eq. (79). The dependence of b_m in δv on the relative speed is neglected in Eq. (80) so that the integral of the kernel with $4\pi|\Delta \mathbf{v}|^2 d|\Delta \mathbf{v}|$ yields the rate given by Eq. (77).

An interesting feature of the three-dimensional kernel, Eq. (80), is that it vanishes for $|\Delta \mathbf{v}| \to 0$. As discussed above, this is expected for $\Delta M \neq 0$ collisions and implies that the corresponding one-dimensional kernel, as given by Eq. (29), has no cusp at $\Delta v = 0$, where Δv is the component of the velocity change along the laser field propagation direction. This one-dimensional kernel is given by

$$W^{d-Q}_{\Delta M=1}(\Delta v) = \gamma^{d-Q}_{\Delta M=1} \frac{4}{\delta v} \int_{(2|\Delta v|/\delta v)}^{\infty} dy \left[\frac{J_2(y)}{y} \right]^2 . \tag{81}$$

Equation (81) yields the kernel $1/e$ width $\Delta v_{1/e} = 1.32 \delta v$.

[1] J. M. Liang, L. A. Spinelli, R. W. Quinn, R. R. Dasari, M. S. Feld, and J. E. Thomas, Phys. Rev. Lett. **55**, 2684 (1985).

[2] J. M. Liang, R. R. Dasari, M. S. Feld, and J. E. Thomas, J. Opt. Soc. Am. B **3**, 506 (1986).

[3] J. M. Liang, J. E. Thomas, R. R. Dasari, and M. S. Feld, Indian J. Phys. **60B**, 318 (1986).

[4] J. M. Liang, Ph.D. thesis, MIT, 1986 (unpublished).

[5] E. W. Smith, J. Cooper, W. R. Chappell, and T. Dillon, J. Quant. Spectrosc. Radiat. Transfer **11**, 1547 (1971); **11**, 1567 (1971).

[6] P. R. Berman, Phys. Rev. A **5**, 927 (1972).

[7] V. A. Alekseev, T. L. Andreeva, and I. I. Sobelman, Zh. Eksp. Teor. Fiz. **62**, 614 (1972) [Sov. Phys.—JETP **35**, 325 (1972)].

[8] S. Stenholm, J. Phys. B **10**, 761 (1977).

[9] W. E. Baylis, Phys. Rev. A **7**, 1190 (1973).

[10] See F. Rohart, B. Segard, and B. Marke, J. Phys. B **12**, 3891 (1979), and references therein.

[11] Ph. Brechignac, J. Chem. Phys. **76**, 3389 (1982).

[12] S. M. Freund, G. Duxbury, M. Romheld, J. T. Tiedje, and T. Oka, J. Mol. Spectrosc. **52**, 38 (1974).

[13] I. D. Abella, N. A. Kurnit, and S. R. Hartmann, Phys. Rev. **141**, 391 (1966).

[14] L. Q. Lambert, A. Compaan, and I. D. Abella, Phys. Rev. A **4**, 2022 (1971).

[15] See, for example, M. Tangigawa, Y. Fukuda, T. Kohmoto, K. Sakuno, and T. Hashi, Opt. Lett. **8**, 620 (1983), and references therein.

[16] Note that for Zeeman rather than Stark tuning, right or left circularly polarized laser light ($\hat{\sigma}_\pm$) could be used. Then there is exact cylindrical symmetry about the laser-beam propagation direction. In this case, spherically averaged kernels are not needed to obtain an evolution equation of the form given by Eq. (5).

[17] P. R. Berman, J. M. Levy, and R. G. Brewer, Phys. Rev. A **11**, 1668 (1975).

[18] J. S. Murphy and J. E. Boggs, J. Chem. Phys. **49**, 3333 (1968).

[19] G. Birnbaum, E. R. Cohen, and J. R. Rusk, J. Chem. Phys. **49**, 5150 (1968).

[20] R. G. Brewer and R. L. Shoemaker, Phys. Rev. Lett. **27**, 631 (1971); J. C. McGurk, C. L. Norris, T. G. Schaltz, E. F. Pearson, and W. H. Flygare, in *Laser Spectroscopy,* edited by R. G. Brewer and A. Mooradian (Plenum, New York, 1974), p. 541.

[21] See, for example, P. R. Berman, T. W. Mossberg, and S. R. Hartmann, Phys. Rev. A **25**, 2550 (1982).

[22] A. Omont, J. Phys. (Paris) **26**, 26 (1965); Prog. Quantum Electron. **5**, 69 (1977).

[23] A. R. Edmonds, *Angular Momentum in Quantum Mechanics* (Princeton University, Princeton, 1974).

[24] See, for example, M. S. Childs, *Molecular Collision Theory* (Academic, New York, 1974).

[25] E. Merzbacher, *Quantum Mechanics* (Wiley, New York, 1970).

[26] H. Jetter, E. F. Pearson, C. L. Norris, J. C. McGurk, and W. H. Flygare, J. Chem. Phys. **59**, 1796 (1973).

[27] K. Gottfried, *Quantum Mechanics* (Benjamin, New York, 1966).

[28] I. S. Gradshteyn and I. M. Ryzhik, *Table of Integrals, Series, and Products* (Academic, New York, 1980).

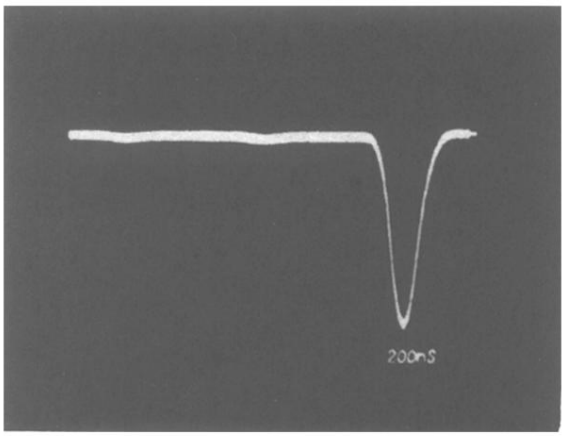

FIG. 5. Echo signal.